

## Monoacylglycerol lipase deficiency in the tumor microenvironment slows tumor growth in non-small cell lung cancer

Melanie Kienzl<sup>a,b</sup>, Carina Hasenoehrl<sup>a</sup>, Kathrin Maitz<sup>a</sup>, Arailym Sarsembayeva<sup>a</sup>, Ulrike Taschler<sup>c</sup>, Paulina Valadez-Cosmes<sup>a</sup>, Oliver Kindler<sup>a</sup>, Dusica Ristic<sup>a</sup>, Sofia Raftopoulou<sup>a</sup>, Ana Santiso<sup>a</sup>, Thomas Bärnthaler<sup>a</sup>, Luka Brcic<sup>d</sup>, Lisa Hahnefeld<sup>e</sup>, Robert Gurke<sup>e,f</sup>, Dominique Thomas<sup>e</sup>, Gerd Geisslinger<sup>e,f</sup>, Julia Kargl<sup>ID a</sup>, and Rudolf Schicho<sup>ID a,b</sup>

<sup>a</sup>Division Of Pharmacology, Otto Loewi Research Center, Medical University Of Graz, Graz, Austria; <sup>b</sup>BioTechMed, Graz, Austria; <sup>c</sup>Institute Of Molecular Biosciences, University Of Graz, Graz, Austria; <sup>d</sup>Diagnostic And Research Institute Of Pathology, Medical University Of Graz, Graz, Austria; <sup>e</sup>Institute Of Clinical Pharmacology, Goethe University, Frankfurt, Germany; <sup>f</sup>Fraunhofer Institute For Translational Medicine And Pharmacology ITMP, Frankfurt, Germany

### ABSTRACT

Monoacylglycerol lipase (MGL) expressed in cancer cells influences cancer pathogenesis but the role of MGL in the tumor microenvironment (TME) is less known. Using a syngeneic tumor model with KP cells (*Kras<sup>LSL-G12D</sup>/p53<sup>fl/fl</sup>*; from mouse lung adenocarcinoma), we investigated whether TME-expressed MGL plays a role in tumor growth of non-small cell lung cancer (NSCLC).

In sections of human and experimental NSCLC, MGL was found in tumor cells and various cells of the TME including macrophages and stromal cells. Mice treated with the MGL inhibitor JZL184 as well as MGL knock-out (KO) mice exhibited a lower tumor burden than the controls. The reduction in tumor growth was accompanied by an increased number of CD8<sup>+</sup> T cells and eosinophils. Naïve CD8<sup>+</sup> T cells showed a shift toward more effector cells in MGL KOs and an increased expression of granzyme-B and interferon- $\gamma$ , indicative of enhanced tumoricidal activity. 2-arachidonoyl glycerol (2-AG) was increased in tumors of MGL KO mice, and dose-dependently induced differentiation and migration of CD8<sup>+</sup> T cells as well as migration and activation of eosinophils *in vitro*.

Our results suggest that next to cancer cell-derived MGL, TME cells expressing MGL are responsible for maintaining a pro-tumorigenic environment in tumors of NSCLC.

### ARTICLE HISTORY

Received 10 June 2021  
Revised 3 August 2021  
Accepted 3 August 2021

### KEYWORDS

Endocannabinoid; 2-AG; cannabinoid receptors; lung cancer; monoacylglycerol lipase; immune cells; CD8<sup>+</sup> T cells

## Introduction

Monoacylglycerol lipase (MGL) was characterized several decades ago as the major enzyme that hydrolyzes monoglycerides into glycerol and fatty acids (rev. in<sup>1</sup>). One of these monoglycerides is 2-arachidonoyl glycerol (2-AG),<sup>2</sup> which has been also identified as an endocannabinoid (rev. in<sup>3</sup>). 2-AG is a full agonist at cannabinoid 1 (CB<sub>1</sub>) and cannabinoid 2 (CB<sub>2</sub>) receptors, thereby causing cannabimimetic effects.<sup>4</sup> MGL contributes to many (patho)physiological conditions, such as pain, food intake, stress, metabolic disorders, addiction, inflammation, and cancer (rev. in<sup>1</sup>). Cannabinoid receptor signaling is terminated through degradation of 2-AG by MGL, which therefore plays, aside from its lipolytic function, a major role in endocannabinoid metabolism.<sup>3</sup> It accounts for around 85% of brain 2-AG hydrolase activity while the remaining part is degraded by enzymes like  $\alpha/\beta$ -hydrolase domain containing (ABHD) 6 and 12.<sup>5</sup> 2-AG, CB<sub>1</sub>/CB<sub>2</sub> and MGL are a chain of key regulators that operate cooperatively within the endocannabinoid system (ECS). Notably, pharmacological inhibition or genetic deletion of MGL results in the accumulation of endogenous 2-AG, but not of arachidonoyl ethanolamide (anandamide; AEA), another well-described endocannabinoid.<sup>6–9</sup> In addition, MGL provides a large

pool of arachidonic acid (AA), from which pro-inflammatory prostaglandins may be generated.<sup>10</sup> This indicates that besides 2-AG, MGL regulates the availability of AA.<sup>8,11</sup>

Apart from metabolizing 2-AG, MGL is known to break down other MGs with different fatty acid chain length and saturation,<sup>12</sup> as well as prostaglandin glycerol esters.<sup>13</sup> The enzyme plays an important role in the intestine where reduced triglyceride secretion after oral fat challenge has been described in MGL deficient mice.<sup>14</sup> MGL also acts as a fatty acid ethyl ester hydrolase and thus may counteract the formation of potentially toxic byproducts of ethanol metabolism.<sup>15</sup>

MGL has lately emerged as an interesting pharmacological target for the treatment of inflammatory diseases and cancer.<sup>16,17</sup> During carcinogenesis, tumor cells shift their energy metabolism toward glycolysis and lipid synthesis.<sup>18</sup> Fatty acids support cancer progression, e.g., by providing building blocks for new membranes. They are also needed for the generation of bioactive lipids that function as signaling molecules.<sup>18</sup> Studies have shown that increased MGL expression/activity in cancer cells drives tumorigenesis through remodeling of fatty acids,<sup>19</sup> suggesting a tumor-promoting role for cancer cell-derived MGL. In keeping with MGL's pro-tumorigenic role, MGL knockdown or treatment with the

MGL inhibitor JZL184 results in reduced proliferation/invasion and increased apoptosis in colorectal cancer (CRC) cell lines.<sup>20,21</sup> Furthermore, treatment with JZL184 reduces metastasis of A549 lung cancer cells in nude mice.<sup>22</sup> High levels of MGL were seen in human melanoma and endometrial cancer samples.<sup>23,24</sup> Other studies showed reduced MGL levels in human samples of CRC<sup>25</sup> and squamous cell carcinoma.<sup>26</sup> In one of these studies, overexpression of MGL in HCT116 CRC cells showed reduced colony formation.<sup>25</sup> In old MGL KO mice, tumors supposedly develop spontaneously, particularly in the lung,<sup>27</sup> suggesting that MGL may rather act as a tumor-suppressor. However, MGL has been considered an unfavorable prognostic factor in primary gastrointestinal stromal tumors<sup>28</sup> and lung adenocarcinoma.<sup>29</sup> At the same time, in pancreatic cancer, no correlation of MGL with survival was detected,<sup>30</sup> indicating that expression of MGL and correlation with tumor aggressiveness in human cancers is still unclear and may depend on the tumor entity and context.

In contrast to our knowledge of the role of MGL in tumor cells, not much is known about the presence and function of MGL in the immune and stromal cells of the tumor microenvironment (TME), in particular, as to how TME-derived MGL influences tumorigenesis. Immune cells express cannabinoid receptors, and they generate/degrade and respond to endocannabinoids, virtually forming an “immune-endocannabinoid system” (rev. in<sup>31,32</sup>). MGL has been detected in macrophages/monocytes and eosinophils (rev. in<sup>32</sup>), and a recent study suggests that MGL is present in tumor-associated macrophages (TAMs) that regulate tumor progression in mouse models of CRC.<sup>33</sup> Using RNAScope<sup>®</sup> in situ hybridization (ISH), we recently showed that T cells (CD3<sup>+</sup>) and macrophages of mouse intestines express MGL.<sup>34</sup>

CD8<sup>+</sup> T cells and eosinophils represent two important anti-tumorigenic immune cell populations in the TME. One of the main roles for CD8<sup>+</sup> T cells in the TME is the killing of tumor cells. CD8<sup>+</sup> cells release cytotoxic granzymes and perforin<sup>35</sup> via recognition of tumor antigen presented by MHC-1.<sup>36</sup> In line with their tumor cell cytotoxicity, increased presence of CD8<sup>+</sup> T cells was reported to correlate with a better outcome in several types of cancer, such as breast<sup>37</sup> and colorectal cancer.<sup>38</sup> The role of eosinophils in the TME is less clear. Although tumor eosinophilia has been correlated with lower tumor progression, the opposite has been also reported.<sup>39</sup> Similar to CD8<sup>+</sup> T cells, their antitumorigenic properties include the degranulation of cytotoxic molecules<sup>40,41</sup> and the recruitment of anti-tumorigenic leukocytes.<sup>42</sup> Because of the presence of cannabinoid receptors in these cells (reviewed in<sup>32</sup>), both CD8<sup>+</sup> T cells and eosinophils can respond to 2-AG. Low MGL expression in tumor tissue could increase 2-AG levels and locally affect the migration and proliferation of these cells; however, this has not been clarified yet.

As the major regulator of 2-AG levels, MGL is critical for CB<sub>1</sub> receptor (de)sensitization and the endocannabinoid tone.<sup>43</sup> By inhibiting MGL, endogenous 2-AG levels increase in a tissue-specific pattern.<sup>6</sup> Tumors also exhibit elevated 2-AG levels, as observed in endometrial cancer.<sup>44</sup> Amongst various endocannabinoids and endocannabinoid-like lipids, only 2-AG has consistently been shown to be increased in experimentally induced tumors (current study).<sup>45,46</sup> Our own

work<sup>47</sup> and a study by Sailer et al.<sup>46</sup> demonstrate that 2-AG levels are increased in plasma of patients with CRC and other types of cancer. Both pro- and anti-inflammatory effects in immune cells have been reported for 2-AG,<sup>31</sup> therefore, elevated levels of 2-AG in tumors could impact immune cell behavior in the TME in opposite ways. Effects of 2-AG on immune cells usually involve cannabinoid receptors, mostly CB<sub>2</sub> (rev. in<sup>31,48</sup>), although CB<sub>1</sub> or cannabinoid receptor independent effects, such as leukotriene biosynthesis and LTB<sub>4</sub> activation might be involved.<sup>49,50</sup>

In the current study, we investigated the role of MGL in the development of NSCLC, with a focus on MGL in the TME. We aimed to identify a potential influence of MGL-expressing TME cells on tumor growth, and on changes in the immune cell landscape of tumors. In particular, we were interested where in the TME MGL is expressed. The TME, specifically the infiltrated immune cell profile, critically determines tumor progression.<sup>51</sup> We used MGL<sup>-/-</sup> knockout (MGL KO) and wild type (WT) mice in a syngeneic NSCLC model in which mice were subcutaneously (s.c.) injected with KP cells (Kras<sup>LSL-G12D</sup>, p53<sup>fl/fl</sup>, established from mouse lung adenocarcinoma) to induce the development of a s.c. tumor. We show that MGL KO mice and mice treated with the MGL inhibitor JZL184 have a lower tumor burden than the WT littermates or vehicle-treated mice, respectively, indicating a pro-tumorigenic role of MGL in NSCLC.

## Materials and methods

### Animal studies and cell culture

All animal experiments were performed in the animal facilities of the Medical University of Graz. C57BL/6J mice were purchased from Charles River. Approval for animal experimental protocols was granted by the Austrian Federal Ministry of Science and Research (protocol number: BMBWF-66.010/0041-V/3b/2018).

MGL KO mice were a gift from Dr. R. Zimmermann<sup>9</sup> from the University of Graz and bred in-house together with wild-type (WT) littermates. The murine KP cell line was isolated from a lung adenocarcinoma of a Kras<sup>LSL-G12D</sup>/p53<sup>fl/fl</sup> mouse at the Fred Hutchinson Cancer Center (Seattle, WA, USA) after intratracheal administration of adenoviral Cre recombinase as described before.<sup>52</sup> The cell line was generously provided by Dr. McGarry Houghton. KP cells were maintained in DMEM with 10% FBS (Life Technologies) and 1% penicillin/streptomycin (P/S, PAA Laboratories) at 37°C and 5% CO<sub>2</sub> in a humidified atmosphere. For the generation of a MGL-overexpressing KP cell line, parental KP cells were transduced with a lentivirus carrying a MGL-CFP-Puro-cassette (KP\_MGL) or a control cassette (KP\_ctrl), which were kindly provided by Dr. C. Heier from the University of Graz.<sup>15</sup> Selection for positive single clones was performed with puromycin (1 µg/ml, Thermo Fisher, A1113803) and confirmed using flow cytometry. Primary human cancer-associated fibroblasts were kindly provided by Dr. K. Leithner from the Medical University of Graz<sup>53</sup> and cultured in DMEM supplemented with 10% FBS and 1% P/S. Cells were starved overnight with serum-free media and 1 or 5 ng/ml TGF-β (Bio-Techne, 7754-BH-005) for 3 days and were used for differentiation.

Mouse primary dermal fibroblasts were cultured according to the manufacturer's protocol (Pellobiotech, Martinsried, Germany).

### **Murine tumor models**

Parental KP cells ( $0.5 \times 10^6$ ) were injected (s.c.) into the right flank of mice. For pharmacological inhibition of MGL, tumor-bearing C57BL/6J wild-type mice were intraperitoneally (i.p.) treated with 16 mg/kg JZL184 (MGL inhibitor, Cayman), once daily, starting one day prior to the injection of tumor cells. For the experiments with MGL-overexpressing cells, either  $0.5 \times 10^6$  KP\_MGL or KP\_ctrl cells were injected (s.c.) into the right flank of C57BL/6J wild-type mice. Tumor growth was monitored during the course of the experiments twice per week using a caliper. Mice were sacrificed after about two weeks, and tumors were subsequently collected, weighted, and measured with a caliper *ex vivo*. Tumor volume was calculated according to the following formula:  $v = \text{length} \times \text{width} \times \text{height} \times \pi/6$ .<sup>40</sup>

### **Single-cell suspensions**

The preparation of single-cell suspensions from tumors was performed as previously described.<sup>40</sup> Using a scalpel, tumors were minced, and digested with DNase I (160 U/ml; Worthington) and collagenase (4.5 U/ml; Worthington) for 15 minutes at 37°C while rotating at 1000 rpm. After brief vortexing, samples were incubated for 10 min before they were passed through a 40  $\mu\text{m}$  cell strainer, washed in PBS +2% FBS, counted, and used for antigen staining.

### **Flow cytometric phenotyping of immune cell populations**

First, single cell suspensions were incubated for 20 min in Fixable Viability Dye (FVD) eFluor<sup>TM</sup> 780 (eBioscience) in the dark to exclude dead cells. After adding 1  $\mu\text{g}$  TruStain<sup>TM</sup> FcX (Biolegend), immunostaining was performed on ice for 30 min (protected from light) with the following antibodies: CD45-AF700 (# 103,128), CD45-BV785 (# 103,149), Ly6C-APC (# 128,015), Ly6C-FITC (# 128,005), Ly6G-PE/Dazzle594 (# 127,648), CD11c-BV605 (# 117,334), CD8-PerCPy5.5 (# 100,734), CD63-PE (# 143,903), PD1-APC (# 135,210), CD62L-BV605 (# 104,438), NKp46-BV510 (# 137,623), CD4-PECy7 (# 100,422), CD4-APC (# 100,516), CD19-PECy7 (# 115,520), CD44-FITC (# 103,005), PD1-BV421 (#135,221), CD62L-BV421 (# 104,436) (all antibodies from Biolegend), and CD11b-BUV737 (# 612,801), F4/80-PE (# 565,410), Siglec-F-PerCPy5.5 (# 565,526), F4/80-BUV395 (# 565,614), CD3-BUV395 (# 563,565), CD4-BUV496 (# 564,667), CD44-BUV737 (# 612,799), Siglec-F-PE (# 562,068) (all antibodies from BD Biosciences). For detection of changes in IFN- $\gamma$  and granzyme-B expression, single-cell suspensions of tumors or spleens ( $2 \times 10^6$  cells per well) were seeded into 96-well U-bottomed plates with RPMI containing 10% FBS, 1% P/S, and GolgiStop (1.5  $\mu\text{l/ml}$ , BD Biosciences) and left for 4 h at 37°C. During that time, they were stimulated with PMA (100 ng/ml, Sigma Aldrich) and ionomycin (1  $\mu\text{g/ml}$ , Sigma Aldrich) or kept without stimulation. After that, surface

staining was performed with CD45-AF700, CD3-BUV395 and CD8-PerCPy5.5, followed by intracellular labeling (BD Cytofix/Cytoperm<sup>TM</sup> Kit) with IFN- $\gamma$ -PECF594 (BD Biosciences, # 562,303) and granzyme-B-AF647 (# 515,406). After staining, cells were washed and fixed using IC Fixation Buffer (eBioscience). Samples were either analyzed on a BD LSRFortessa<sup>TM</sup> or BD Canto<sup>TM</sup> flow cytometer with FACSDiva software (BD Biosciences). Analyses and compensation were performed with Flowjo software (TreeStar). Fluorescence minus-one-samples were used to define gates. See *Supplementary figure S1* for gating strategies.

### **RNA extraction and qRT-PCR**

RNA extraction from tissue was carried out in TRIzol (Life Technologies). For RNA extraction from cultured cells, RNeasy Kit (Qiagen) was used. Samples were treated with either a DNA-free DNA Removal Kit (Invitrogen) or RNase-Free DNase set (Qiagen). One  $\mu\text{g}$  of RNA was reversely transcribed with the High-Capacity cDNA Reverse Transcription Kit (Applied Biosystems). Quantification of gene expression by RT-qPCR was performed with SsoAdvanced Universal SYBR Green Supermix (Bio-Rad). Primers were acquired from Eurofins (*Supplementary table 1*) or Bio-Rad (*Supplementary table 2*).  $\Delta\text{Cq}$ - and  $\Delta\Delta\text{Cq}$ -methods were used for the assessment of relative gene expression.<sup>54</sup>

### **Differentiation of bone marrow-derived eosinophils (BMDEs)**

Bone marrow was isolated from C57BL/6J wild-type mice, and eosinophils were differentiated as previously described.<sup>40</sup> In short, after lysis of erythrocytes with ddH<sub>2</sub>O and 10xPBS, cells were cultured in BMDE-RPMI, i.e. RPMI+20% HyClone FBS (GE Healthcare; # 10,309,433), 25 mM HEPES (Thermo Fisher; # 15,630-080), 1xnon-essential amino acids (Thermo Fisher; # 11,140-035), 1 mM sodium pyruvate (Thermo Fisher; #11,360-039), 1% P/S and 50  $\mu\text{M}$  beta-mercaptoethanol (Sigma-Aldrich; M3148) supplemented with 100 ng/ml FLT3L (PreproTech; # 250-31 L) and 100 ng/ml stem cell factor (PreproTech; # 250-03) for four days at 37°C and 5% CO<sub>2</sub>. After that, the medium was changed to BMDE-RPMI supplemented only with 10 ng/ml IL-5 (Bio-Techne). Every fourth day, cells were transferred to a new flask, and a fresh medium was added every other day. Fully differentiated BMDEs were used for assays on day 14.

### **Ca<sup>2+</sup> flux in eosinophils**

BMDEs were treated with 2  $\mu\text{M}$  of Fluo-3 AM in the presence of 0.02% pluronic F-127 for 1 hr at room temperature and protected from light.<sup>55</sup> Then, 1  $\mu\text{M}$  of the CB<sub>2</sub> antagonist SR144528 or EtOH as control was added for the last 10 min. BMDEs were subjected to baseline measurement for 60 sec and additionally stimulated with increasing concentrations of 2-AG (Tocris) or DMSO (vehicle). Changes in intracellular Ca<sup>2+</sup> were determined as an increase in the 530/30 nm channel on a BDCalibur flow cytometer.

### Isolation of lymphocytes from spleen

CD3<sup>+</sup> and CD8<sup>+</sup> T cells were isolated from spleens of MGL KO mice and their WT littermates with EasySep<sup>TM</sup> mouse CD8<sup>+</sup> T cell/T cell isolation kit according to the manufacturer's protocol (Stemcell).

### BMDE and CD8<sup>+</sup> T cell migration assay

Migration assays were performed using 5 µm Transwell plates (Corning), as previously described.<sup>56</sup> In brief, BMDEs and negatively isolated murine CD8<sup>+</sup> T cells were seeded in the upper well (at  $1 \times 10^5$  or  $1.5 \times 10^5$  cells per well, respectively), and increasing concentrations of 2-AG were used as a chemoattractant for 1 or 4 h at 37°C, respectively. DMSO was used as vehicle. SR144528 or EtOH (control) was used as a pretreatment (1 µM, 10 min at room temperature). CCL19 (Biolegend) was used as a positive control for CD8<sup>+</sup> T cell migration. Enumeration of cells migrating to the lower well was performed on a BDCanto<sup>TM</sup> flow cytometer (BD Biosciences).

### T cell differentiation and proliferation assay

Isolated murine T cells were seeded into 96-well U-bottom plates ( $1.5 \times 10^5$  cells per well, pre-coated with 5 µg/ml ULTRA-LEAF<sup>TM</sup> anti-mouse CD3 antibody (Biolegend)) with X-VIVO<sup>TM</sup> 15 medium (Szabo-Scandic) containing 1% P/S, 2 nM L-glutamine, 50 µM β-mercaptoethanol, 25 mM HEPES, 50 U/ml mIL-2, 1x non-essential amino acids (Thermo Fisher; # 11,140-035), 1 mM sodium pyruvate (Thermo Fisher; # 11,360-039), and ULTRA-LEAF<sup>TM</sup> anti-mouse CD28 antibody 1 µg/ml (Biolegend). T cells were then treated with different concentrations of 2-AG following pretreatment with 1 µM SR144528 or vehicle for 30 min. To determine T cell proliferation, cells were pre-loaded with 5 µM eFluor<sup>TM</sup> 450 cell proliferation dye (Invitrogen) for 10 min at 37°C. After 4 days of incubation at 37°C, T cells were harvested and staining was performed as described above.

### In situ hybridization (ISH) and immunofluorescence

Tumors were fixed in acid-free phosphate-buffered 10% formaldehyde solution (Roti<sup>®</sup>-Histofix 10%, pH7) for 16–24 h at room temperature, and further processed for paraffin embedding according to standard procedures. Tissue was cut in 5 µm sections, baked at 60°C for 1 hr, de-waxed and rehydrated. ISH was performed according to the manufacturer's protocol and as recently published.<sup>34</sup> In brief, three ZZ probes for MGL (targeting bases 703–849 of NM\_001166251.1) (BaseScope<sup>TM</sup> RED kit; Advanced Cell Diagnostics [ACD]) were used to detect the corresponding mRNAs in tumors. Sections with tumor tissue were treated with H<sub>2</sub>O<sub>2</sub> for 10 min and target retrieval was performed using the Brown FS3000 food steamer for 15 min. Each step was followed by washes in distilled water. The sections were then digested with Protease IV at 40°C for 20 min, washed, followed by incubation with the corresponding probes at 40°C for 2 h and stained using FastRed. Samples from MGL

KO and WT mice were put on one slide for comparison. MGL KO mice lacked expression of MGL outside of the engrafted KP tumor cells. The specificity of the MGL probe is also published elsewhere.<sup>34</sup>

ISH and immunofluorescence were performed on 4 µm sections of the human lung adenocarcinoma formalin-fixed paraffin-embedded samples obtained from the Biobank of the Medical University of Graz. mRNA was detected using an anti-human MGL probe (targeting bases 566–1530 of NM\_007283.6 (RNAScope 2.5 HD Assay-RED kit, ACD; cat. # 539,151)). Ethical approval was obtained from the Institutional Review Board of the Medical University of Graz (EK-numbers: 30–105 ex 17/18). All procedures involving human participants were in accordance with the ethical standards of the institutional and/or national research committee and with the 1964 Helsinki Declaration and its later amendments or comparable ethical standards. Informed consent was obtained from all subjects involved in the study.

Antibodies against cytokeratin (1:200; Dako # ZO0622), F4/80 (1:500; Cell Signaling # 70,076) or CD163<sup>+</sup> (1:500; Abcam # ab182422), CD3<sup>+</sup> (1:500; Novus # NB6001441SS), CD11b (1:100; Novus # NB11089474), fibroblast-specific protein (FSP) (1:100; Millipore #72,274), von Willebrand factor (vWF) (1:400; Abcam # ab6994), α-SMA (1:100; Abcam # ab5694), were used to determine tumor cells and cell types of the immune/stromal TME co-localizing with MGL mRNAs. After ISH, tissue sections were first blocked in 0.1 M PBS containing 0.3% Triton X-100 and 5% goat serum (Sigma-Aldrich). Primary antibodies were applied in 0.1 M PBS containing 0.3% Triton X-100 and 1% goat serum over night at 4°C. As the second antibody, Alexa Fluor<sup>®</sup> 488-labeled goat anti-rabbit IgG (1:500; Jackson Immuno Research; #111-546-144) was used. Sections were also equally processed without primary antibodies as a negative control. Afterward, sections were mounted with Vectashield<sup>®</sup> (containing DAPI) (Vector Laboratories) and images were taken by an Olympus IX70 fluorescence microscope (Olympus) connected with a Hamamatsu ORCA-ER digital camera (Hamamatsu Photonics K.K., Japan). Images were processed with Olympus CellSense<sup>®</sup> 1.17 imaging software (Olympus). The contrast, brightness and color balance of images were adjusted using Corel Photo Paint<sup>®</sup>.

### LC-MS analytics of endocannabinoids and other lipids

Endocannabinoids, endocannabinoid-like substances, DGs, TGs and other lipids from mouse tumor and adjacent white adipose tissue were determined using liquid chromatography in combination with tandem mass spectrometry (LC-MS/MS) and high-resolution mass spectrometry (LC-HRMS), respectively. Details about the used equipment, materials, method parameters and a full list of analyzed analytes can be found in the *Supplementary materials S2 (LC-MS analytics)*.

Tissue was homogenized prior to lipid extraction using wet grinding in a Precellys 24 (Bertin Instruments, Montigny-le-Bretonneux, France) at 10°C. The tissue homogenates had a concentration of 0.05 mg/µL in ethanol:water (1:3, v/v), and 10 zirconium dioxide balls were added for the grinding. For quantification of endocannabinoids and related substances,

tissue homogenates equaling 2 mg of tissue and a 1:50 dilution in ethanol:water (1:3, v/v) were extracted after filling up the sample volume to 200  $\mu$ L with ethanol:water (1:3, v/v). Quantitation of endocannabinoids and related compounds was achieved as described previously with a shortened gradient and reduced source temperature of 400°C to enhance sensitivity of 2-oleoyl glycerol (2-OG).<sup>57</sup> Due to the shortened gradient, OEA and its isomer vaccenic acid ethanolamide (VEA) were not separated and were, therefore, quantified as a sum parameter.

1-arachidonoyl glycerol (1-AG), 2-AG, arachidonoyl ethanolamide (AEA), oleoyl ethanolamide (OEA), palmitoyl ethanolamide (PEA) and 2-OG were extracted from 200  $\mu$ L sample volume using liquid-liquid-extraction by adding 20  $\mu$ L of internal standards in acetonitrile, 20  $\mu$ L acetonitrile and 400  $\mu$ L ethyl acetate: hexane (9:1, v/v). After mixing and centrifugation at 4°C for 3 min, the upper organic layer was transferred and dried under a nitrogen stream at 45°C. Before analysis, samples were dissolved in 50  $\mu$ L acetonitrile. The LC-MS/MS measurement included separation on an Agilent 1290 Infinity II UHPLC system with an Acquity UPLC BEH C18 column (100  $\times$  2.1 mm, 1.7  $\mu$ m, Waters, Eschborn, Germany) and measurement on a QTrap 6500+ (Sciex, Darmstadt, Germany) using an ESI Turbo-V-source with negative ion source voltage. Data were acquired using Analyst software v1.7.1 and further analyzed with MultiQuant software v 3.0.2. Acceptance criteria and quality assurance measures were applied as described previously.<sup>57</sup> The lower and upper limits of quantification for all analytes can be found in the *Supplementary materials S2*.

The lipid screening using LC-HRMS was performed as described previously with a shortened gradient, which is further described in the *Supplementary materials S2*.<sup>58</sup> Additionally, oleic acid was quantified within this analysis. Lipids were extracted using a modified MTBE extraction protocol.<sup>59</sup> A volume of 10  $\mu$ L tissue homogenate ( $\equiv$  0.5 mg tissue) was mixed with 75  $\mu$ L of internal standards in methanol, 10  $\mu$ L of oleic acid-d9 in methanol, 250  $\mu$ L MTBE and 60  $\mu$ L 50 mM ammonium formate. The mixture was vortexed for 1 min and centrifuged for 5 min at 20,000 g at room temperature. After transfer of the upper organic phase, the aqueous phase was re-extracted with 100  $\mu$ L of a mixture of MTBE: methanol: water (10:3:2.5, v/v/v, upper phase). The combined organic phases were dried under a stream of nitrogen at 45°C and reconstituted in 100  $\mu$ L methanol before LC-HRMS analysis. For the calibration standards and quality control samples for oleic acid, 20  $\mu$ L of ethanol:water 1:3 (v/v) was mixed with 20  $\mu$ L standard/qc solution in methanol containing 0,1% BHT, 55  $\mu$ L methanol, 10  $\mu$ L oleic acid-d9 in methanol, 250  $\mu$ L MTBE and 60  $\mu$ L 50 mM ammonium formate and extracted as described above.

The measurement was performed using a Vanquish Horizon UHPLC system coupled to an Exploris 480 (both Thermo Fisher Scientific, Dreieich, Germany) applying a Zorbax RRHD Eclipse Plus C8 column (1.8  $\mu$ m 50  $\times$  2.1 mm ID, Agilent, Waldbronn, Germany). Both ionization modes were used with a scan range from 180 to 1500 m/z and a mass resolution of 120.000 combined with data-dependent acquisition at 15.000 mass resolution with a full

scan every 0.6 s. For verification of the system stability, the first twelve samples were pooled and replicates injected at the start, at the end of a run as well as after every 10<sup>th</sup> sample. For data acquisition and peak integration, XCalibur software v4.4 and TraceFinder software v5.1 were used with a mass tolerance of 5 ppm.

In a semi-targeted approach, 318 lipids were evaluated and results were normalized to one internal standard per lipid class. These lipids were identified using exact mass  $\pm$  5 ppm, isotope ratio and comparison of MS/MS fragmentation pattern with LipidBlast database.<sup>60</sup> A relative standard deviation below 20% for the quality control samples was used as acceptance criteria for the lipid screening. Oleic acid was quantified in negative ionization mode full scan as hydrogen-loss and the same quality assurance and acceptance criteria as for the endocannabinoids were applied.<sup>57</sup>

### Statistical analysis

GraphPad Prism 6.1 (GraphPad® Software) was used to perform statistical analyses for *in vitro* and *in vivo* experiments. Gaussian distribution was tested by using Shapiro-Wilk normality test. Statistically significant differences between two experimental groups were determined using unpaired student's *t*-tests, multiple *t*-tests or two-way ANOVA with the indicated *post hoc* test for corrections of multiple comparisons. To compare three or more groups, one-way ANOVA was used with the indicated *post hoc* test for corrections of multiple comparisons. Statistical analysis for not normally distributed data was performed using non-parametric Mann-Whitney tests and Kruskal-Wallis test with Dunn's multiple comparison test. Correlations between tumor weight/volume and MGL, ABHD6 or 12 expressions were determined using Pearson's correlation coefficient (*r*) and Spearman's correlation coefficient *rho* (*r<sub>s</sub>*).

Lipid species data was analyzed in R (Version 4.0.3) using Welch's *t*-test, and plots were drawn with the pheatmap-package (Raivo Kolde, 2019. pheatmap: Pretty Heatmaps. R package version 1.0.12. <https://CRAN.R-project.org/package=pheatmap>). Colors indicate the up- (red) or down (blue) regulation of each lipid.

*P* values < .05 were considered significant and denoted with 1, 2 or 3 asterisks when lower than 0.05, 0.01 or 0.001, respectively.

## Results

### MGL-deficiency in cells of the TME inhibits tumor growth in a syngeneic NSCLC model

In recent publications, reduced lung cancer cell invasiveness was detected after treatment with an MGL inhibitor.<sup>22,29</sup> We, therefore, treated KP cell tumor bearing C57BL/6J mice with the MGL inhibitor JZL184 (or vehicle) first to investigate whether systemic blockade of MGL affects primary tumor growth (Figure 1a). As a result, the inhibitor slowed tumor progression (Figure 1b) and caused a significant reduction in tumor weight and volume (Figure 1c). To validate whether JZL184 truly inhibited MGL activity, we performed a monoacylglycerol hydrolase (MGH)

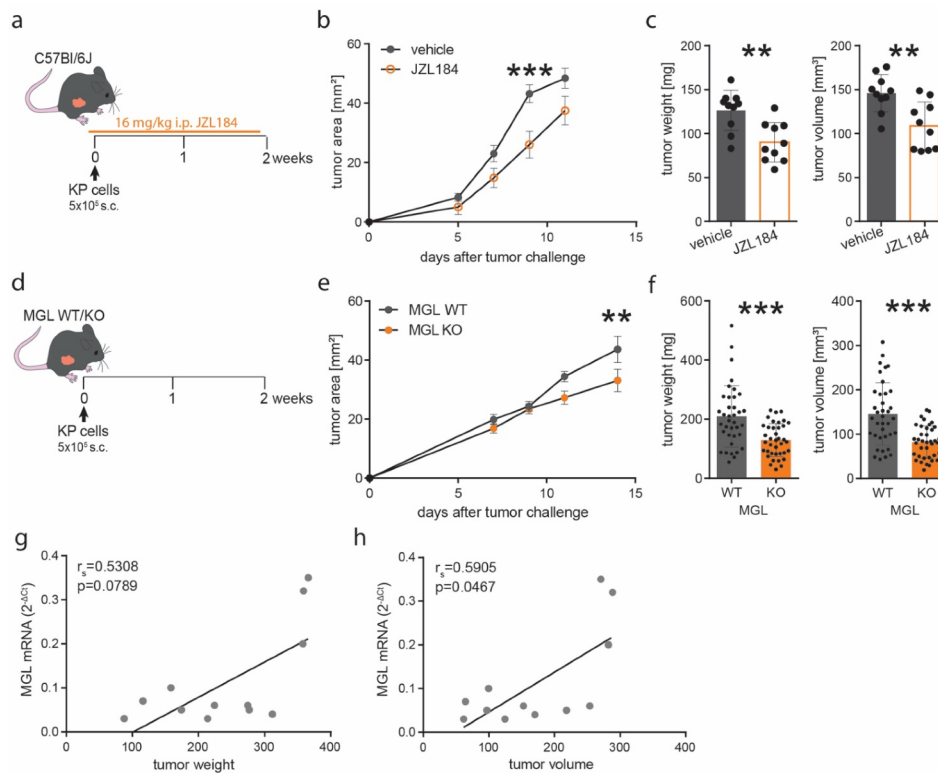


**Figure 1.** Pharmacological inhibition of MGL and genetic MGL deficiency in cells of the TME inhibit tumor growth in a model of non-small cell lung cancer. **(a)** C57Bl/6J wild-type mice were injected subcutaneously (s.c.) with  $5 \times 10^5$  KP lung adenocarcinoma cells (time point 0) and tumors were allowed to grow for 12 days. Mice were additionally injected intraperitoneally (i.p.) either with 16 mg/kg of the MGL inhibitor JZL184 (or vehicle) once daily, starting the day before tumor cell injections. **(b)** Tumor development was monitored over the course of the experiment. Data indicate means  $\pm$  SEM. One representative experiment is shown.  $n = 10$ . **(c)** *Ex vivo* tumor weight and volume were evaluated at the end of the experiment. One representative experiment is shown. Data indicate means  $\pm$  SEM.  $n = 10$ . **(d)** MGL wild type (WT) and knockout (KO) mice were injected s.c. with  $5 \times 10^5$  KP lung adenocarcinoma cells (time point 0) and tumors were allowed to grow for 15 days. **(e)** Tumor development was monitored during the course of the experiment. Data indicate means  $\pm$  SEM. One representative experiment is shown.  $n = 9$ –10. **(f)** After 15 days, mice were sacrificed, and tumor weight and volume were measured *ex vivo*. Data indicate means  $\pm$  SEM and were pooled from four independent experiments.  $n = 37$ –38. Correlations between MGL mRNA expression and tumor weight **(g)** or volume **(h)**. Two representative experiments were pooled.  $n = 12$ . Statistical differences were assessed using two-way ANOVA with Tukey's multiple comparison test, student's *t*-test or Mann-Whitney test. Correlation was determined by using Spearman's correlation coefficient rho ( $r_s$ ). \*\* $p < .01$ , \*\*\* $p < .001$

activity assay in protein lysates of the liver from vehicle- and JZL184-treated mice, demonstrating the systemically inhibiting effect of JZL184 on MGL activity (*Supplementary figure S3a*). JZL184 treatment had no direct effect on tumor cells and did not influence tumor cell viability (evaluated as CD45<sup>+</sup> cells; *Supplementary figure S3b*) or proliferation (*Supplementary figure S3c and d*) *in vivo*.

As the role of MGL has not yet been investigated in the TME of NSCLC, we aimed to find out whether tumor infiltrating cells that were deficient of MGL (thus creating a MGL deficient TME) would be sufficient to reduce tumor growth. We injected KP cells into the flank of MGL KO and WT mice (*Figure 1d*). The growth of tumors was monitored over 2 weeks and similar to the effect of JZL184, we found reduced tumor growth in the MGL KO vs. WT mice (*Figure 1e*). *Ex vivo* analysis of tumor weight and volume showed an approximate 40% reduction of tumor size in MGL KO mice (*Figure 1f*). mRNA expression of MGL in tumors from WT mice positively correlated with tumor size (*Figure 1g, h*). mRNA expression of other monoglyceride hydrolases like ABHD6 (recently suggested as a tumor-driver in NSCLC<sup>61</sup>) and ABHD12 showed no significant correlations (*Supplementary figures S3e-h*).

### MGL deficiency in cells of the TME favors an anti-tumorigenic immune cell profile

We next investigated whether the reduced tumor size that we observed in MGL KO mice was accompanied by changes in the immune cell profile of the TME (*Figure 2a-g*). In comparison to WT mice, flow cytometry of tumor-infiltrating leukocytes in the MGL KO mice revealed significant increases in the number of eosinophils (*Figure 2c*) and CD8<sup>+</sup> T cells (*Figure 2e*), indicating a potential shift to an anti-tumorigenic environment. However, no differences were detected in CD4<sup>+</sup> T, overall T, NK, NKT and B cells (*Figure 2d*). In WTs, the relative abundance of naïve CD4<sup>+</sup> and CD8<sup>+</sup> T cells were higher than in KO mice (*Figure 2f*), while in KO mice, the relative abundance of effector CD8<sup>+</sup> T cells was higher than in WTs (*Figure 2g*). The expression of the inhibitory checkpoint receptor PD-1 on tumor-infiltrating CD4<sup>+</sup> and CD8<sup>+</sup> T cells was increased in tumors from MGL KO mice suggesting increased immune activity of these cells (*Figure 2h*). Expression levels of granzyme-B (*Figure 2i, j*) and IFN- $\gamma$  (*Figure 2k, l*) were increased in tumor-infiltrating CD8<sup>+</sup> T cells of MGL KO vs. WT mice, indicating enhanced tumoricidal activity of CD8<sup>+</sup> T cells in MGL KO mice.

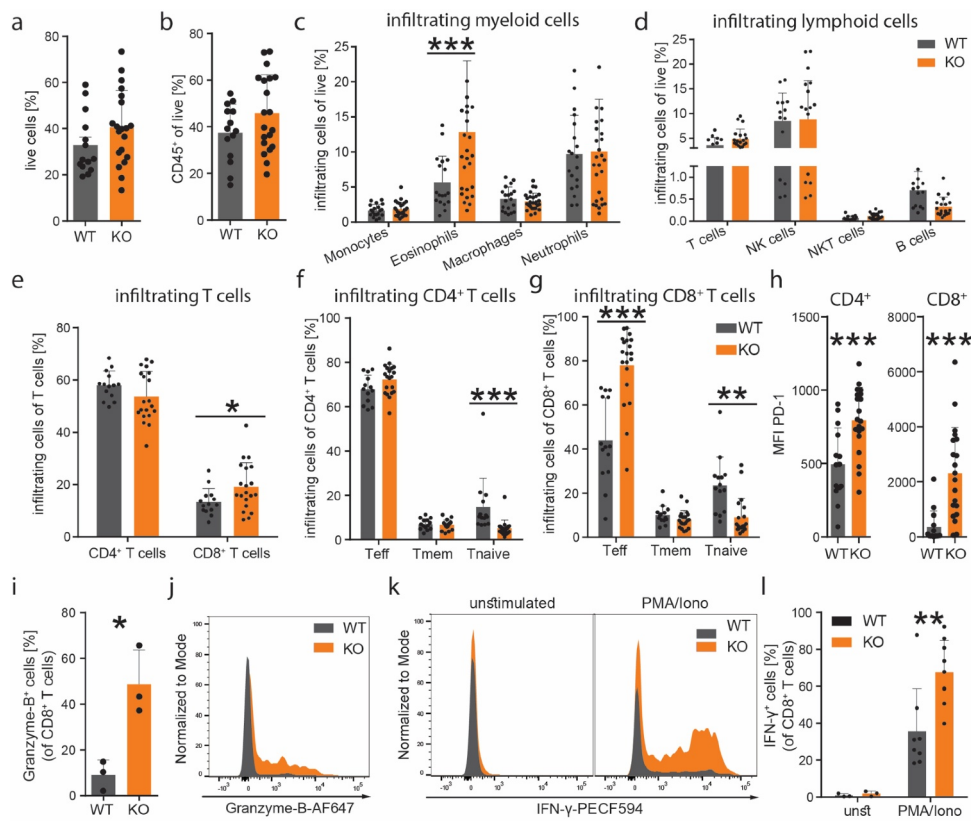


**Figure 2.** MGL deficiency in cells of the TME favors an anti-tumorigenic immune cell profile. (a–g) Flow cytometric analysis of single cell suspensions of KP cell tumors from MGL wild type (WT) and knockout (KO) mice (effector T cells, *Teff*; memory T cells, *Tmem*; naïve T cells, *Tnaive*). Data were pooled from two or three independent experiments;  $n = 14$ – $20$ ; mean values  $\pm$  SD. (h) Median fluorescence intensity (MFI) of PD-1 on CD4 and CD8<sup>+</sup> T cells is shown. Data were pooled from two independent experiments;  $n = 14$ – $20$ ; mean values  $\pm$  SD. (i) The graph shows flow cytometric analysis of granzyme-B expression of tumor infiltrating CD8<sup>+</sup> T cells from MGL WT and KO mice as well as a (j) representative histogram. Data indicate means  $\pm$  SD,  $n = 3$ . (k) Representative histograms of IFN- $\gamma$  expression before (unstimulated, *unst*) and after phorbol 12-myristate 13-acetate/ionomycin (*PMA/Iono*) stimulation of tumor infiltrating CD8<sup>+</sup> T cells. (l) Quantitative analysis of tumor infiltrating CD8<sup>+</sup> T cells showing increased expression of IFN- $\gamma$  in the MGL KO mice after *ex vivo* PMA/Iono stimulation. Data indicate means  $\pm$  SD,  $n = 9$ – $10$ . Statistical differences were assessed by using student's *t*-test or Mann-Whitney test and multiple *t*-tests. \* $p < .05$ ; \*\* $p < .01$ ; \*\*\* $p < .001$ .

### MGL is expressed in tumor cells and various cells of the TME

Our first results showed that MGL deficiency in cells of the TME resulted in a lower tumor burden accompanied by changes in the TME. Since previous data showed that MGL expression in TME macrophages had an influence on tumor progression,<sup>33</sup> we were interested, in which cells of the TME of our NSCLC model MGL were expressed.

We used ISH technique with a specific probe against MGL combined with immunofluorescence (we have tested the specificity of this probe in MGL KO mice previously<sup>34</sup>). In tumors of MGL WT mice, only 40% of DAPI-stained nuclei, that stained for the tumor cell marker cytokeratin, colocalized with adjacent MGL mRNA ISH signals (Figure 3a), indicating that MGL mRNA was also expressed by TME cells. Within the TME, we detected MGL mRNA in F4/80-positive macrophages (Figure 3b), fibroblast specific protein (FSP)-positive tumor-associated fibroblasts (Figure 3c), endothelial cells (Figure 3d), but, particularly, in  $\alpha$ -SMA positive cells (Figure 3e). Of note, primary fibroblasts from NSCLC patients and dermal fibroblasts from C57BL/6 mice differentiated by TGF- $\beta$  also expressed MGL mRNA in cell cultures, hence

confirming our findings (see *Supplementary figures S4a and b*). CD3<sup>+</sup> T cells did not express MGL mRNA in the tumors (Figure 3f). Around 20% of cytokeratin positive cells stained for MGL mRNA (Figure 3g). As expected, cells in the TME from tumors of MGL KO mice were devoid of MGL mRNA expression and staining for MGL mRNA in these mice was, therefore, only observed in tumor cells (see *Supplementary figures S4c–h*). MGL RT-qPCR in tumor samples of WT mice was higher than in KO mice (Figure 3h). The qPCR data in the MGL KO mice indicated that MGL was expressed in KP cells *in vivo* thus confirming our ISH data. KP cells kept in culture only marginally expressed MGL mRNA (*Supplementary figure S4i*), and equally, expression of ABHD6 mRNA was low (*Supplementary figure S4i*). MGL and ABHD6 mRNAs showed equally high expression in tumors of WT mice (Figure 3i). There were no differences in ABHD6 expression between MGL KO and WT mice (*Supplementary figure S4j*). At the same time, ABHD12 showed highly elevated expression in MGL WT tumors (Figure 3i) and cultured KP cells (*Supplementary figure S4i*), but no changes were seen between MGL KO and WT tumors (*Supplementary figure S4k*).

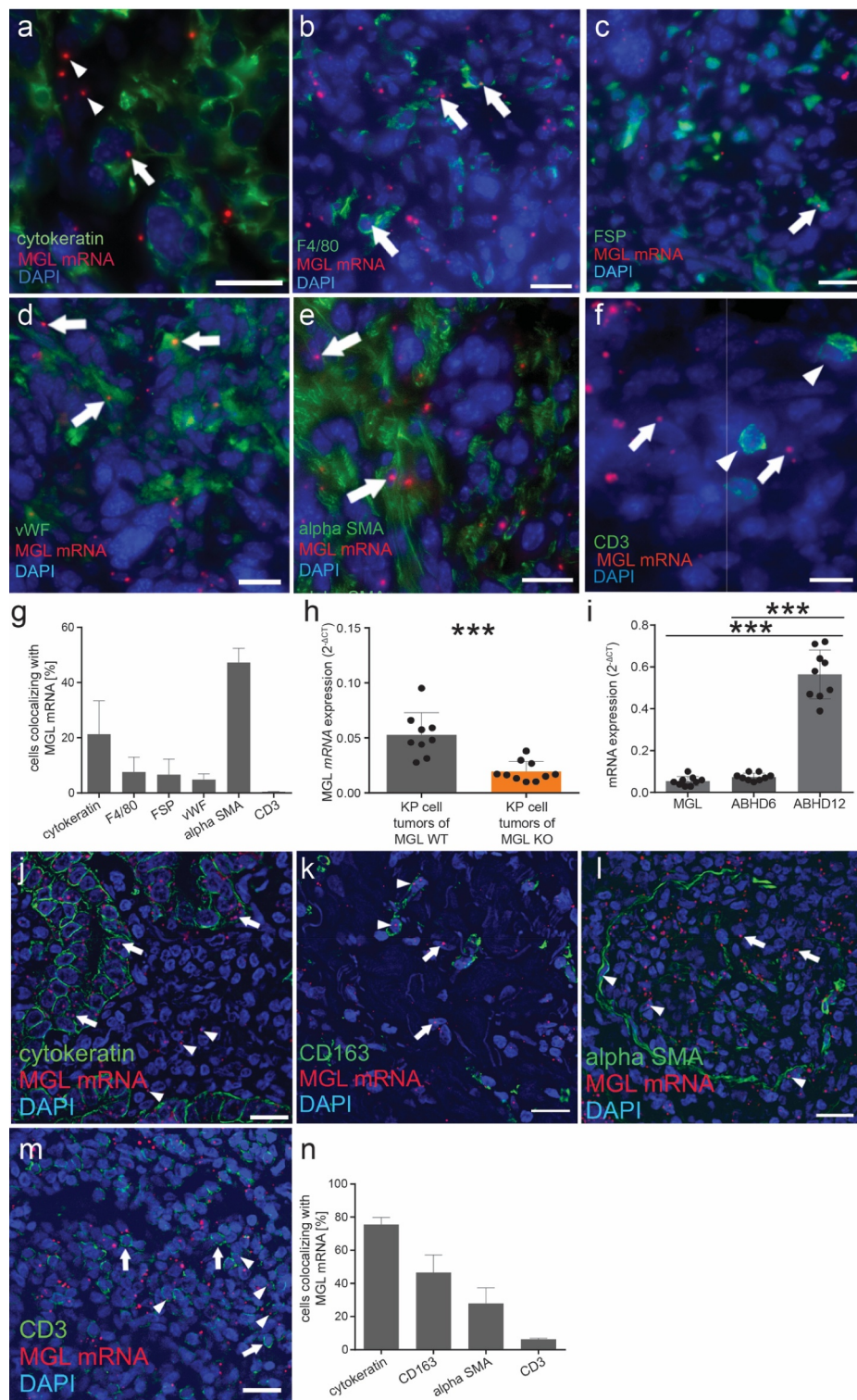


**Figure 3.** In situ hybridization (ISH) of MGL mRNA in KP cell tumors of MGL wild type (WT) mice. **(a)** In MGL WT mice with KP cell tumors, MGL transcripts can be seen in tumor cells (*arrow*; cytokeratin used as a tumor cell marker), and also outside cytokeratin-positive cells (*arrowheads*). MGL mRNA colocalizes with cells of the TME (*arrows*) such as with **(b)** macrophages (F4/80; ~7%), **(c)** cells expressing fibroblast specific protein (FSP; ~6%), **(d)** endothelial cells (von Willebrand factor – vWF; ~5%), and **(e)** to a large part with (alpha)  $\alpha$ -SMA positive fibroblasts; ~47%. **(f)** MGL mRNA expression (*arrows*) was not observed in CD3<sup>+</sup> T cells (*arrowheads*). **(g)** Graph showing % of MGL mRNA colocalization with indicated cell populations in tumor sections. Cells from three different tumor sections were used for quantification. Between 60 and 250 cells/section were evaluated for colocalization. Data show means + SD. **(h)** Relative MGL mRNA expression in lysates of KP cell tumors from MGL WT and KO mice.  $n \geq 9$ . Data indicate means + SD of one representative experiment. One-way ANOVA with Tukey's multiple comparison test. \*\*\* $p < .001$  **(i)** Relative mRNA expression of MGL, ABHD6 and ABHD12 in lysates of KP cell tumors from WT mice. Data show means + SD.  $n = 9$ . One-way ANOVA with Tukey's multiple comparison test. \*\*\* $p < .001$ . **(j)** Similar to KP cell tumors in mice, sections of human adenocarcinoma show MGL mRNA ISH signals in tumor cells (using cytokeratin as a tumor cell marker; *arrows*) and in the TME (*arrowheads*). **(k)** MGL mRNA signals are visible in CD163<sup>+</sup> macrophages (*arrowheads*) next to other cells of the tumor (*arrows*). **(l)** Also in human lung adenocarcinoma, MGL mRNA colocalizes with (alpha)  $\alpha$ -SMA positive fibroblasts (*arrowheads*) next to other cells of the tumor (*arrows*). **(m)** Unlike in the KP cell tumors of mice, colocalization of MGL mRNA was seen in some CD3<sup>+</sup> positive T cells (*arrowheads*). *Arrows* denote CD3<sup>+</sup> positive T cells without MGL mRNA expression. **(n)** % of MGL mRNA colocalization with indicated cell populations in tumor sections. Sections from two patients with lung adenocarcinoma were used for quantification. Between 75 and 500 cells/section were evaluated for colocalization. Data show means + SD. Calibration bars: 20  $\mu$ m

In sections of human lung adenocarcinoma, most tumor cells expressed MGL mRNA (75%) (Figure 3j). In addition, we detected MGL mRNA in CD163<sup>+</sup> macrophages (46%) and in  $\alpha$ -SMA positive cells (28%) (Figure 3 k,l). Unlike in the KP cell tumors of mice, the human samples showed MGL mRNA expression in some CD3<sup>+</sup> T-cells (6%) (Figure 3m and 3n).

### ***In vitro*, 2-AG shifts CD8<sup>+</sup> T cells toward a T effector phenotype and activates eosinophils in a CB<sub>2</sub> dependent manner**

MGL hydrolyzes monoglycerides (MGs), and in that function it may affect 2-AG and also other lipid levels. We, therefore, measured MGs, endocannabinoids, endocannabinoid-like lipids and free fatty acids (FAs) in tumors of MGL deficient and WT mice, first focusing on changes of endocannabinoids and MGs in tumor tissues. Mass spectrometric measurements revealed increased levels of 2-AG and 2-OG in tumors of MGL KO as compared to WT mice (Figure 4a). Next to 2-AG, AEA and palmitoylethanolamide (PEA) were increased in tumors of JZL184-treated vs. vehicle-treated control mice (Supplementary figure S5a). When comparing 2-AG levels of KO and WT tumor tissue vs. tumor-adjacent white adipose tissue, increased levels were detected in KP tumor tissue, indicating a tumor-specific rise of 2-AG that was significantly higher in tumors of MGL KO mice (Supplementary figure S5b).

Second, as MGL has been reported to regulate FA levels in aggressive cancer cells,<sup>19</sup> we investigated whether FAs were altered in our tumor models. However, we did not detect alterations in FA contents but noted increased triglyceride levels in the MGL KO tumors instead. Many lipid species described as being altered in human lung cancer tissue, such as phosphatidylcholines (PCs,<sup>62</sup>) and lysophosphatidylcholines (LPCs,<sup>63</sup>), were found increased in tumors of MGL KO mice (Supplementary figure S5c).

Since we had found increased levels of 2-AG in the tumors of MGL KO vs. WT and JZL184-treated mice (Figure 4a and Supplementary figure S5a), we investigated whether 2-AG could play a role in the change of the infiltrating immune cell populations in MGL KO mice (specifically CD8<sup>+</sup> T cells and eosinophils) and/or tumor cell proliferation. We first investigated the role of 2-AG on differentiation, migration, and proliferation of CD8<sup>+</sup> T cells *in vitro*. Based on our finding that CD44/CD62L-expression revealed a shift to an increase in infiltrating CD8<sup>+</sup> T effector cells into tumors of MGL KO mice, as compared to WTs, we checked CD44 expression on polyclonal-stimulated T cells *in vitro*. We observed an increased CD44 expression in CD8<sup>+</sup> T cells from MGL KOs compared to WTs that was not sensitive to CB<sub>2</sub> inhibitor SR144528 treatment (Figure 4b). To confirm an involvement of 2-AG, we additionally treated T cells isolated from MGL WT spleens with different concentrations of 2-AG and recorded a dose-dependent increase in CD44<sup>+</sup> CD8<sup>+</sup> T cells (Figure 4c).

As a next step, we isolated T cells from MGL WT and KO mice and investigated migration in response to increasing concentrations of 2-AG (chemoattractant) in

a Transwell plate. We identified dose-dependent migration of CD8<sup>+</sup> T cells toward 2-AG (Figure 4d). Since there was no significant difference in the migratory potential between MGL WT and KO CD8<sup>+</sup> T cells, we continued our experiments with WT cells. Here, the additional treatment with SR144528 showed a reduced migration compared to control (EtOH)-treated cells (Figure 4e), suggesting the involvement of a CB<sub>2</sub> dependent mechanism in migration.

We also investigated whether the proliferation of CD8<sup>+</sup> T cells could be affected by 2-AG. However, incubation of T cells with different concentrations of 2-AG did not change their proliferative behavior (Supplementary figures S6a and a). Although 2-AG was described to reduce the growth of pancreatic cancer cells *in vitro*,<sup>64</sup> we failed to see the effects of 2-AG on KP tumor cell proliferation and viability *in vitro* (Supplementary figures S7a and b).

In addition to CD8<sup>+</sup> T cells, we isolated eosinophils (which are known to express CB<sub>2</sub><sup>56,65</sup>) from bone marrow cells of WT mice and differentiated them into bone marrow-derived eosinophils (BMDEs). MGL expression was not detected in eosinophils within tumors (data not shown); therefore, the following experiments were performed in WT cells only. BMDEs were used on day 14 with purity and viability of about 93% and 94%, respectively (Supplementary figure S8), and we tested the chemotactic potential of 2-AG. BMDEs migrated toward 2-AG in a dose-dependent manner (Figure 4f). Migration was suppressed after pre-treatment with 1  $\mu$ M of CB<sub>2</sub> inhibitor SR144528, corroborating previous findings<sup>56</sup> (Figure 4f, representative dot plots are shown in Figure 4g). We also wanted to know whether 2-AG could induce Ca<sup>2+</sup> flux in murine eosinophils via CB<sub>2</sub>, as previously described for human eosinophils.<sup>56</sup> Ca<sup>2+</sup> flux was dose-dependently increased in BMDEs of MGL WT mice when stimulated with 2-AG (Figure 4h). Similar to the chemotactic effect of 2-AG, pre-treatment with 1  $\mu$ M of SR144528 reduced Ca<sup>2+</sup> signals almost to baseline values (Figure 4h-i).

Taken together, our *in vitro* data indicate that 2-AG activates eosinophils and promotes differentiation in CD8<sup>+</sup> T cells, supporting the observed *in vivo* effects.

### ***WT mice injected with MGL-overexpressing KP cells showed increased tumor growth***

In addition to cells of the TME (Figure 3b-e), MGL is expressed in KP tumor cells *in situ* (Figure 3a), but is hardly detectable in cultures of KP cells *in vitro* (Supplementary figure S4h). To investigate whether tumor cell-expressed MGL affects tumor growth and the TME landscape in our model, we generated KP cells overexpressing MGL, which were lentivirally transduced either with a MGL-encoding (KP\_MGL) or a control plasmid (KP\_ctrl). CFP (present in the control and the MGL-encoding plasmid) was used for sorting successfully transduced cells (Supplementary figure S9a). MGL overexpression in the transduced KP cell line was confirmed by qPCR and MGH activity assay (Supplementary figure S9b-c). WT mice were injected s.c. with either the MGL-overexpressing

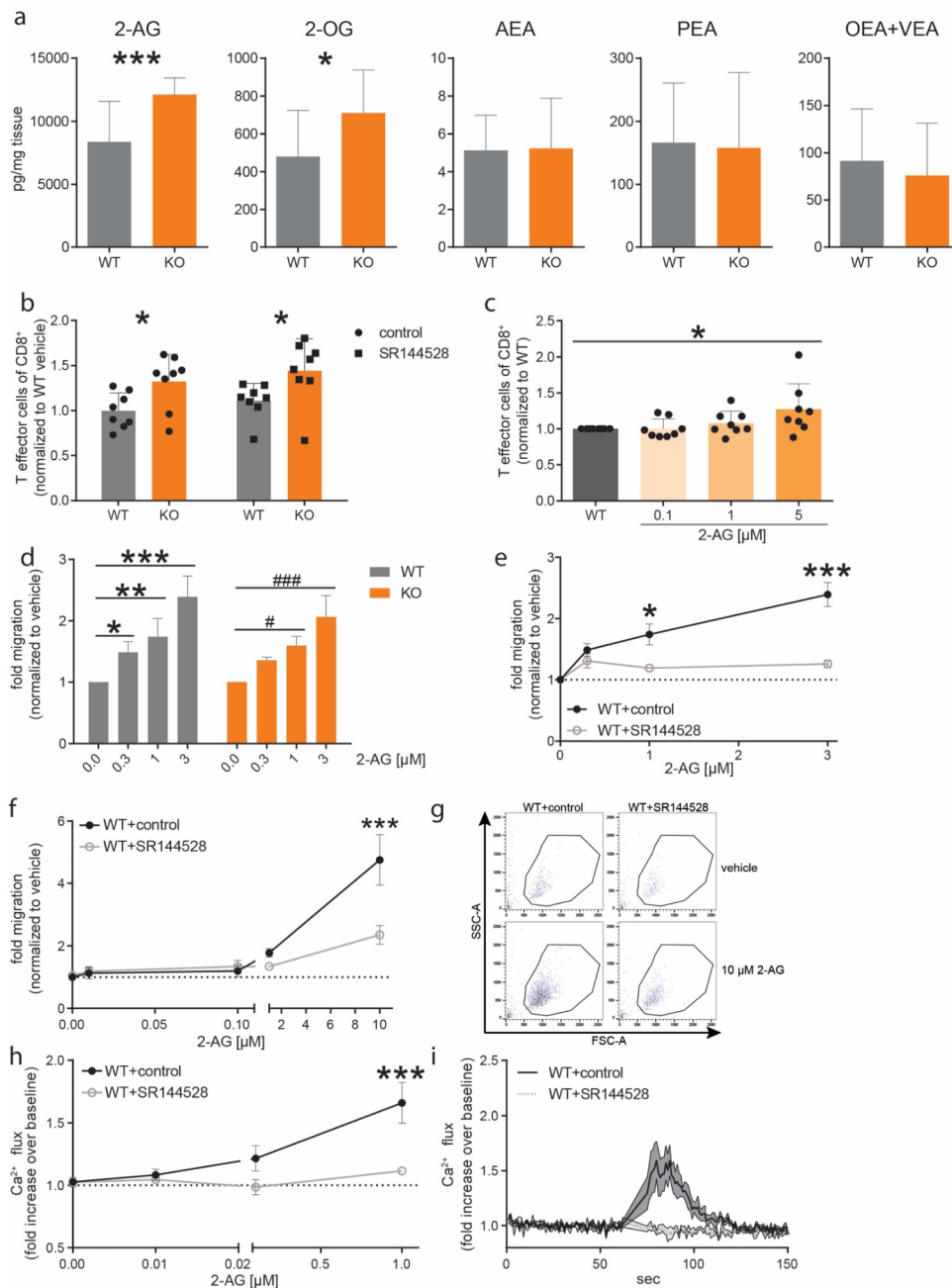


**Figure 4.** 2-AG shifts CD8<sup>+</sup> T cells toward a T effector phenotype and activates eosinophils *in vitro*. **(a)** Tumors were snap frozen in liquid nitrogen and the tissue homogenate was subsequently analyzed by mass spectrometry. Graphs show lipid levels of MGL WT and KO tumors ( $n \geq 12$ ). **(b)** T cells were isolated from the spleen of WT and MGL KO mice and incubated for 3 days with anti-CD3/CD28-antibodies as well as pre-treated (30 min) with 1  $\mu$ M of the CB<sub>2</sub> antagonist SR144528 or control (<0.05% EtOH). **(c)** T cells isolated from WTs were treated with anti-CD3/CD28-antibodies and with increasing concentrations of 2-AG (or vehicle [ $<0.05\%$  DMSO]). T cell differentiation was detected by flow cytometry. Data show means + SD from three independent experiments normalized to CD44 expression of WT vehicle-treated T cells.  $n = 8$ . **(d)** CD8<sup>+</sup> T cells were isolated from spleens of MGL WT and KO mice and were allowed to migrate toward different concentrations of 2-AG or vehicle in a Transwell plate and counted by flow cytometry.  $n = 3$ . **(e)** CD8<sup>+</sup> T cells of WT mice were additionally pre-treated with 1  $\mu$ M of SR144528 for 10 min (or control). Statistical difference of migrated (toward 2-AG) CD8<sup>+</sup> T cells WT+control compared to WT+SR144528. **(f)** Bone marrow-derived eosinophils (BMDEs) from WT (C57BL/6J) mice were allowed to migrate toward different concentrations of 2-AG or vehicle in a Transwell plate and enumerated by flow cytometry. The BMDEs were incubated with 1  $\mu$ M of SR144528 (or control). Data are shown as means  $\pm$  SEM from three independent experiments.  $n = 3-4$ . **(g)** Representative dot plots of migrated BMDEs. Numbers indicate BMDEs counted for high with flow cytometry. **(h)** BMDEs from WT mice were labeled with Fluo-3-AM and flow cytometry was used to detect changes in the Ca<sup>2+</sup> flux. BMDEs were pre-treated with 1  $\mu$ M SR144528 or control. Subsequently, BMDEs were stimulated with different concentrations of 2-AG or vehicle only. Results represent fold increase in Ca<sup>2+</sup> flux over baseline. Data are shown as means  $\pm$  SEM from three individual experiments.  $n = 3-4$ . Statistical difference of WT +control vs. 1  $\mu$ M SR144528 treated BMDEs. **(i)** Time course of Ca<sup>2+</sup> flux in BMDEs stimulated with 1  $\mu$ M 2-AG. BMDEs were either pretreated with 1  $\mu$ M SR144528 or control. After baseline measurement (60 s), 2-AG was added to induce Ca<sup>2+</sup> flux. Data are shown as means  $\pm$  SEM or + SD from three independent experiments.  $n = 3-4$ . Statistical differences were assessed by using two-way ANOVA with Tukey's or Sidak's post hoc test, student's *t*-test and one-way ANOVA with Dunnett's multiple comparison test. \* $p < .05$ ; \*\* $p < .01$ ; \*\*\* $p < .001$ .

or the control KP cell line and tumor growth was monitored for about 14 days (Figure 5a). In general, tumors in

these experiments were smaller than tumors in Figure 1 (tumors with non-transfected KP cells), which may have

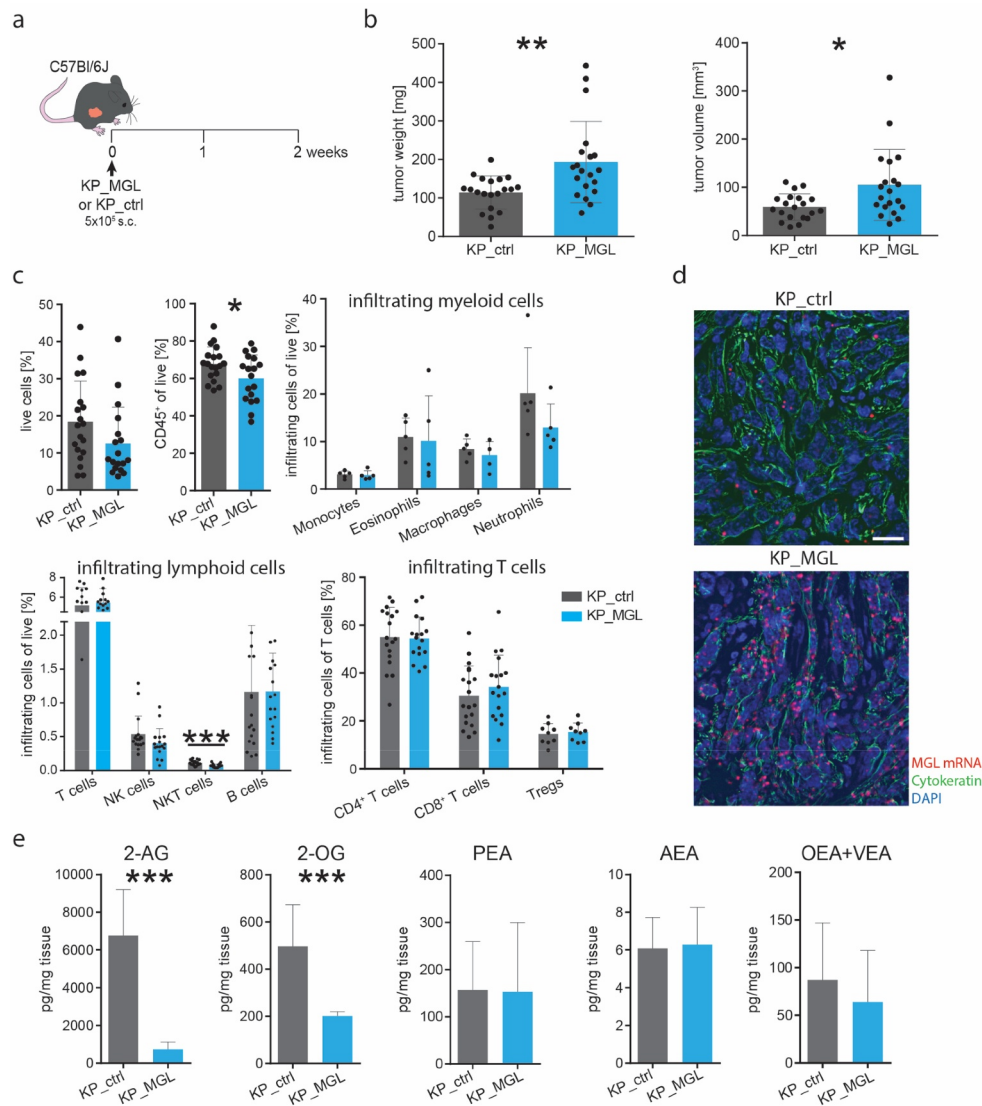


**Figure 5.** Increased tumor growth in WT mice injected s.c. with MGL-overexpressing KP cells. **(a)** KP cells were lentivirally transduced to overexpress MGL (KP\_MGL) or a control plasmid (KP\_ctrl), and afterward injected s.c. into the flank of C57BL/6J wild-type mice. **(b)** Mice were sacrificed and *ex vivo* tumor weight and volume were measured. Data indicate means + SD. Data were pooled from two independent experiments,  $n = 20$ . **(c)** Flow cytometric analysis of single cell suspensions of KP cell tumors. Data were pooled from two independent experiments;  $n = 18$ –19; for myeloid cells only one experiment is shown ( $n = 5$ ). **(d)** Representative pictures of KP\_MGL/ctrl tumors after *in situ* hybridization for MGL (MGL, red; cytokeratin, green; DAPI, blue). Calibration bar: 20  $\mu\text{m}$  **(e)** Lipid levels in KP-MGL overexpressing (KP\_MGL) and control (KP\_ctrl) tumors. Data indicate means + SD,  $n = 8$ –12, pooled from two independent experiments. Statistical differences were assessed by using two-way ANOVA with Sidak's post hoc test, student's *t*-test or Mann-Whitney test and multiple *t*-tests. \* $p < .05$ ; \*\* $p < .01$ ; \*\*\* $p < .001$ .

been due to the immunogenicity of CFP.<sup>66</sup> Analysis of *ex vivo* tumor weight and volume demonstrated significantly increased tumor burden in mice with the overexpressing MGL KP tumor cells (Figure 5b). Using BrdU-staining, we excluded that differences in the proliferation of the cell lines *per se* could have been responsible for the increase in tumor growth (Supplementary figure S9d).

Flow cytometric analysis of single-cell suspensions of tumors from MGL-overexpressing vs. control mice showed reduced infiltration of CD45<sup>+</sup> and NKT cells. However, no changes in the T and B cell profiles, nor in infiltrating myeloid cell populations (Figure 5c). The results suggest that next to TME-expressed MGL, tumor cell-expressed MGL may also promote tumor growth in our model though with minor impact on the TME immune cell

profile. Increased MGL expression in tumor cells was also detected by ISH for MGL combined with immunofluorescence of cytokeratin (tumor cell marker) (Figure 5d). Endocannabinoid levels were measured with mass spectrometry and showed significantly reduced 2-AG and 2-OG levels in MGL-overexpressing KP tumors compared to control (Figure 5e). Lipid screening revealed differences in various lipid species between KP\_MGL and KP\_ctrl tumors (Supplementary figure S10). The lipid profile of MGL overexpressing tumors was less altered as compared to tumors from MGL KO mice suggesting that MGL located in TME cells may have a critical influence on the composition of the tumor lipid profile and maybe on the generation of procarcinogenic precursors. No increase of FAs was seen in MGL overexpressing tumors.

## Discussion

Despite a decline since 2008, lung cancer is estimated to cause more deaths than breast, prostate, colorectal, and brain cancers combined.<sup>67</sup> NSCLC comprises the majority of all lung cancers. Although significant advances have been achieved with new forms of treatment, such as immunotherapy, NSCLC remains challenging to treat, calling out for a better understanding of the TME's role in this type of cancer.<sup>68</sup>

Lately, the immune cell landscape of NSCLC has been characterized, describing reactive T cells and neutrophils as potentially important players of NSCLC carcinogenesis.<sup>69</sup> Since components of the endocannabinoid system are widely present in immune cells (rev. in<sup>32</sup>), we wanted to address the question whether the 2-AG degrading enzyme MGL located in the TME contributes to NSCLC carcinogenesis. A link between endocannabinoid degradation and NSCLC has previously been reported in an immunocompromised mouse model demonstrating a reduction in tumor growth and metastasis by FAAH inhibitors.<sup>70,71</sup> Furthermore, decreased invasion and metastasis of lung cancer cells were detected upon MGL inhibitor treatment in athymic mice.<sup>22</sup> Other than these reports, only cannabinoids and their receptors have been studied in lung cancer cells and in *in vivo* lung cancer models (e.g.<sup>72–74</sup>). A study by Xiang et al. has focused on MGL inside the TME and investigated the role of MGL in macrophages and its impact on tumor growth in gastrointestinal cancer mouse models showing a significant impact of MGL on cancer progression.<sup>33</sup> Data are otherwise contradictory whether MGL promotes tumor growth or acts as a tumor suppressor.

### The MGL/2-AG axis in the TME affects lung cancer

We applied a cell line generated from a mouse lung adenocarcinoma in a syngeneic NSCLC tumor model and studied tumor

growth, MGL expression, and alterations in immune cell populations of the TME (summarized in Figure 6).

We could show that tumors with a MGL-deficient TME were smaller than tumors with a MGL positive TME. We also observed higher levels of 2-AG in MGL KO vs. WT mice tumors, most likely because of an absence of MGL expression in the TME of the KOs. Higher levels in tumors vs. normal tissue have been frequently observed for 2-AG<sup>46</sup> (also reviewed in<sup>32</sup>), and confirmed in our study. Furthermore, Qiu et al. have shown an anti-tumorigenic effect of 2-AG on tumor progression in a model of pancreatic cancer,<sup>64</sup> suggesting that the MGL/2-AG axis indeed could be critical in the pathogenesis of cancer. Our data also showed that MGL mRNA expression levels positively correlated with tumor burden in the NSCLC model (Figure 1h). In line with that, low expression of MGL was associated with increased survival in hepatocellular carcinoma.<sup>75</sup> Unlike other findings,<sup>61</sup> no evidence for a correlation of ABHD6 with tumor size was detected in our study, whereas the high expression of ABHD12 suggests that this enzyme could be a monoglyceride hydrolase in tumor cells next to MGL with a potential role in NSCLC pathogenesis.

Concerning MGL mRNA expression in tumor cells *in vitro*, we observed very low expression in the cultured KP cells while MGL mRNA was visibly expressed in tumor cells *in situ*, suggesting that MGL RNA expression is upregulated once KP tumor cells grow inside the body. Thus, *in situ* tumor cells as well as TME cells, many of them  $\alpha$ -SMA-positive fibroblasts, were found to express MGL indicating that degradation of 2-AG and potential use of AA for the synthesis of other mediators like prostaglandins<sup>10,11</sup> could occur in cancer as well as in TME cells. We corroborated MGL in tumor and TME cells in sections of human lung adenocarcinoma by ISH/immunofluorescence, and in lung fibroblasts from NSCLC patients *in vitro*.

### MGL and 2-AG affect differentiation and tumoricidal activity of CD8<sup>+</sup> T cells

The deficiency of MGL in cells of the TME had a significant impact on the immune cell profile, which was shifted to a more anti-tumorigenic profile. Significant increases were observed for cytotoxic CD8<sup>+</sup> T cells and eosinophils in MGL KO vs. WT mice tumors. A more detailed investigation of CD8<sup>+</sup> T cells revealed that they were also more active (higher levels of granzyme B and IFN- $\gamma$ ) and that 2-AG may have direct effects on the conversion of T naïve into T effector cells. This is of high interest, as reduced T effector cells<sup>76</sup> and a potential dysregulation of T lymphocytes with reduced IFN- $\gamma$  expression were detected in NSCLC patients.<sup>77</sup> Thus, the impact on the CD8<sup>+</sup> T cell population may represent an important mechanism against tumorigenesis generated by MGL deficiency in the TME. 2-AG has already been described to induce changes in the immune cell composition of the TME, leading to an increase in myeloid-derived suppressor cells (MDSCs) in a model of pancreatic cancer.<sup>64</sup> In contrast to our findings, CD4<sup>+</sup> and CD8<sup>+</sup> T cells were not affected in this model.<sup>64</sup> We were able to confirm a role

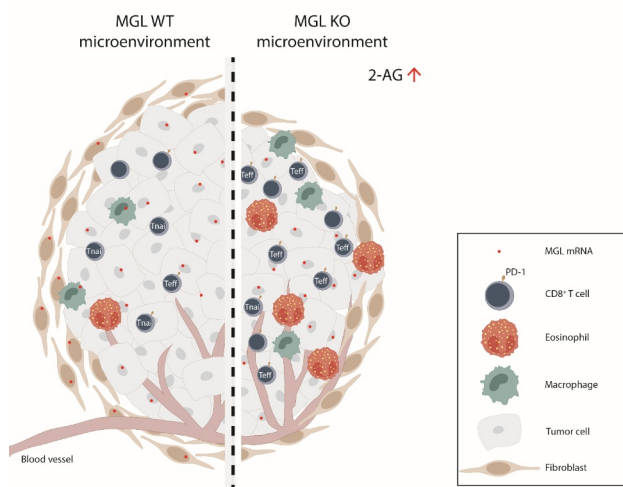


**Figure 6.** Deficiency of MGL in the tumor microenvironment (TME) alters the immune cell infiltrate in tumors of a non-small cell lung cancer model. Summary of differences observed in the TME cell landscape of MGL wild type (WT) and MGL knockout (KO) mouse tumors. An increase in levels of 2-AG in tumors from MGL KO mice is accompanied by increased infiltration of eosinophils and CD8<sup>+</sup> T cells. Furthermore, the number of effector cells (Teff) and the expression of PD-1<sup>+</sup> on CD8<sup>+</sup> T cells are increased. The altered TME cell profile in the MGL KO mice may favor tumor reduction. (Tnaïv= naïve T cells).

of 2-AG in CD8<sup>+</sup> T cell migration *in vitro*, suggesting that 2-AG may have contributed to the higher number of CD8<sup>+</sup> T cells in KP tumors of MGL KO mice *in vivo*.

We also observed increased PD-1 expression on CD4<sup>+</sup> and CD8<sup>+</sup> T cells in our study, which could be a consequence of high T cell activity against antigens in tumors of MGL KO mice.<sup>78</sup> When comparing PD-1<sup>+</sup> and PD-1<sup>-</sup> CD8<sup>+</sup> T cells in an adoptive T-cell therapy study, authors found that only PD-1<sup>+</sup> CD8<sup>+</sup> T cells could control tumor progression, and that anti-PD-L1 therapy further enhanced this effect<sup>79</sup> adding translational value to our findings.

Collectively, our data on the immune cell infiltrate in our NSCLC model indicate that MGL derived from TME cells may suppress infiltration, differentiation and activity of CD8<sup>+</sup> T cells during tumor progression in NSCLC. MGL in TME cells is, therefore, likely responsible for maintaining a tumor progressive environment.

### Direct effects of 2-AG on immune cells

Since increased 2-AG levels were measured in tumors of MGL KO and JZL184-treated mice, we hypothesized a direct role of 2-AG signaling in tumor development. As CB<sub>1</sub> receptors are desensitized in MGL KOs or mice chronically treated with a high dosage of JZL184,<sup>7,80</sup> we excluded the involvement of CB<sub>1</sub> in our experiments. We, therefore, concentrated our *in vitro* experiments on CB<sub>2</sub> and observed CB<sub>2</sub> dependent effects in the differentiation of CD8<sup>+</sup> T cell phenotypes and activation of eosinophils by 2-AG. However, we cannot exclude that 2-AG may have also acted via leukotriene receptors by rapid hydrolysis and leukotriene biosynthesis as previously shown.<sup>50</sup> Human leukocytes are known to contain several hydrolases other than MGL and could hydrolyze 2-AG.<sup>81</sup> In contrast to previous findings of an anti-proliferative effect on e.g. pancreatic cancer cells by 2-AG,<sup>64</sup> we failed to see a direct influence of 2-AG on tumor cell proliferation and apoptosis *in vitro*. As to eosinophils, they are known to exhibit pro-tumorigenic and many anti-tumorigenic properties dependent on the types of cancer (rev. in<sup>82</sup>). In human NSCLC, eosinophils are usually present at low levels (0.3% of all immune cells),<sup>83</sup> however, we counted higher numbers of eosinophils in the MGL KOs of our model (around 12%), which could have contributed to an anticarcinogenic effect.

### MGL overexpressed in KP cells contributes to tumor growth

As described above, MGL is expressed in KP tumors *in vivo*, but it is hardly present in KP cells *in vitro*. To identify if tumor cell-derived MGL might contribute to changes in tumor growth and in the TME profile, we used lentiviral transduction to create a MGL-overexpressing KP cell line. Tumor growth was increased in MGL-overexpressing KP cells *in vivo*. Our data are in line with a study by Nomura et al., who showed increased MGL expression in aggressive cancer cells, and enhanced tumorigenic behavior when MGL was overexpressed in non-aggressive cancer cells.<sup>19</sup> Thus, together with another study showing that overexpression of MGL in nasopharyngeal

carcinoma cells increased their metastatic potential,<sup>84</sup> MGL in KP tumor cells (next to TME-derived MGL) also governs tumor progression. However, since we failed to detect changes in the number of T cells and eosinophils (though we noted a decrease in NKT cells) in the immune cell infiltrate of the TME of MGL overexpressing tumors, tumor cell-derived MGL may have less importance than TME-derived MGL in regulating the TME immune landscape.

### Lipids display distinct profiles in tumors of MGL WTs vs. KOs, and in mice with MGL overexpressing tumor cells

Many lipid species evaluated in our study were increased in MGL KO mice vs. wild-types, such as species of LPC, PCs and sphingomyelins. Some of these lipids have been found decreased in lung cancer, for instance PC (18:4/3:0) and LPC (18:0,18:1,18:2).<sup>62,63,85</sup> However, at the moment, we can only speculate whether an increase in these lipids could have contributed to the reduced tumor growth in the MGL KO mice. No differences in the content of FAs were observed between MGL overexpressing and normal tumors suggesting that MGL overexpressed in tumor cells may not provide FAs for procarcinogenic lipid mediators in our model.

In conclusion, we could show that MGL is present in cells of the TME in a model of NSCLC and that it impacts the tumor growth and the landscape of the TME. Identifying major mechanisms for a favorable response to immune checkpoint therapy,<sup>86</sup> such as increased CD8<sup>+</sup> T cell infiltration and IFN- $\gamma$  production, ablation of MGL in the TME may highlight a new strategy for potential adjuvant therapy. Together with the fact that a MGL inhibitor reduced tumor growth in NSCLC suggests that MGL could be an interesting target in NSCLC anti-tumor therapy.

### Acknowledgments

Ph.D. candidate Melanie Kienzl received funding from BioTechMed Graz, Austria. PhD candidates SR and AS received funding from the Austrian Science Fund (FWF; doctoral programs: DK-MOLIN W1241). MK, PVC, OK, SR, and AS were trained within the frame of the PhD Program *Molecular Medicine* of the Medical University of Graz. Work in the lab of JK is supported by the OENB Anniversary Fund (17584) and a FFG-Bridge 1 grant (871284). T.B. is a recipient of the FWF Schroedinger Fellowship (J4547). The primary human cancer-associated fibroblasts were a gift from Dr. Katharina Leithner. Dr. Christoph Heier from the University of Graz kindly provided the MGL-CFP-Puro and control cassette carrying plasmids. We are grateful to Veronika Pommer, Sabine Kern, Yannick Schreiber, Alena Sens and Carlo Angioni for their excellent technical assistance.

### Author contributions

MK, CH, JK and RS designed the experiments and supervised the study. MK, CH, KM, AS, UT, PVC, SR, DR, LB and TB participated in all the *in vivo* and *in vitro* experiments, collected data, and analyzed the results. MK and OK did the statistical evaluation and the correlations. UT performed the MGH assays, TB the ISH and immunofluorescence experiments. LB provided the human samples. LH, RG, and DT were responsible for the mass spectrometry experiments. MK, CH, JK, GG and RS interpreted the data and provided technical support. MK, JK, and RS participated in the writing of the manuscript. All authors critically revised and commented on the manuscript.

## Disclosure statement

The author(s) report no conflict of interest.

## Funding

The work was supported by the Austrian Science Fund (FWF): grants P30144 (RS), P33325 (RS), KLIF887 (RS), P31638 (UT).

## ORCID

Julia Kargl  <http://orcid.org/0000-0002-0870-0816>

Rudolf Schicho  <http://orcid.org/0000-0002-5726-4731>

## References

- Grabner GF, Zimmermann R, Schicho R, Taschler U. Monoglyceride lipase as a drug target: at the crossroads of arachidonic acid metabolism and endocannabinoid signaling. *Pharmacol Ther.* 2017;175:35–46. doi:10.1016/j.pharmthera.2017.02.033.
- Dinh TP, Freund TF, Piomelli D. A role for monoglyceride lipase in 2-arachidonoylglycerol inactivation. *Chem Phys Lipids.* 2002;121(1–2):149–158. doi:10.1016/S0009-3084(02)00150-0.
- Lu H-C MK. Review of the endocannabinoid system. *Biological Psychiatry: Cognitive Neuroscience and Neuroimaging.* Aug 1 2020. doi: 10.1016/j.bpsc.2020.07.016
- Sugiura T. Physiological roles of 2-arachidonoylglycerol, an endogenous cannabinoid receptor ligand. *Biofactors.* 2009;35(1):88–97. doi:10.1002/biof.18.
- Blankman JL, Simon GM, Cravatt BF, Comprehensive A. A comprehensive profile of brain enzymes that hydrolyze the endocannabinoid 2-Arachidonoylglycerol. *Chem Biol.* 2007;14(12):1347–1356. doi:10.1016/j.chembiol.2007.11.006.
- Long JZ, Li W, Booker L, Burston JJ, Kinsey SG, Schlosburg JE, Pavón FJ, Serrano AM, Selley DE, Parsons LH, et al. Selective blockade of 2-arachidonoylglycerol hydrolysis produces cannabinoid behavioral effects. *Nat Chem Biol.* 2009;5(1):37–44. doi:10.1038/nchembio.129.
- Schlosburg JE, Blankman JL, Long JZ, Nomura DK, Pan B, Kinsey SG, Nguyen PT, Ramesh D, Booker L, Burston JJ, et al. Chronic monoacylglycerol lipase blockade causes functional antagonism of the endocannabinoid system. *Nat Neurosci.* 2010;13(9):1113–1119. doi:10.1038/nn.2616.
- Nomura DK, Hudak CSS, Ward AM, Burston JJ, Issa RS, Fisher KJ, Abood ME, Wiley JL, Lichtman AH, Casida JE. Monoacylglycerol lipase regulates 2-arachidonoylglycerol action and arachidonic acid levels. *Bioorg Med Chem Lett.* 2008;18(22):5875–5878. doi:10.1016/j.bmcl.2008.08.007.
- Taschler U, Radner FPW, Heier C, Schreiber R, Schweiger M, Schoiswohl G, Preiss-Landl K, Jaeger D, Reiter B, Koefeler HC, et al. Monoglyceride lipase deficiency in mice impairs lipolysis and attenuates diet-induced insulin resistance. *J Biol Chem.* 2011;286(20):17467–17477. doi:10.1074/jbc.M110.215434.
- Nomura DK, Morrison BE, Blankman JL, Long JZ, Kinsey SG, Marcondes MCG, Ward AM, Hahn YK, Lichtman AH, Conti B, et al. Endocannabinoid hydrolysis generates brain prostaglandins that promote neuroinflammation. *Science.* 2011;334(6057):809–813. doi:10.1126/science.1209200.
- Grabner GF, Eichmann TO, Wagner B, Gao Y, Farzi A, Taschler U, Radner FPW, Schweiger M, Lass A, Holzer P, et al. Deletion of monoglyceride lipase in astrocytes attenuates lipopolysaccharide-induced neuroinflammation. *J Biol Chem.* 2016;291(2):913–923. doi:10.1074/jbc.M115.683615.
- Vandevoorde S, Saha B, Mahadevan A, Razdan RK, Pertwee RG, Martin BR, Fowler CJ. Influence of the degree of unsaturation of the acyl side chain upon the interaction of analogues of 1-arachidonoylglycerol with monoacylglycerol lipase and fatty acid amide hydrolase. *Biochem Biophys Res Commun.* 2005;337(1):104–109. doi:10.1016/j.bbrc.2005.09.015.
- Savinainen JR, Kansanen E, Pansar T, Navia-Paldanius D, Parkkari T, Lehtonen M, Laitinen T, Nevalainen T, Poso A, Levonen A-L, et al. Robust hydrolysis of prostaglandin glycerol esters by human monoacylglycerol lipase (MAGL). *Mol Pharmacol.* 2014;86(5):522–535. doi:10.1124/mol.114.094284.
- Douglass JD, Zhou YX, Wu A, Zadrogra JA, Gajda AM, Lackey AI, Lang W, Chevalier KM, Sutton SW, Zhang S-P, et al. Global deletion of MGL in mice delays lipid absorption and alters energy homeostasis and diet-induced obesity. *J Lipid Res.* 2015;56(6):1153–1171. doi:10.1194/jlr.M058586.
- Heier C, Taschler U, Radulovic M, Aschauer P, Eichmann TO, Grond S, Wolinski H, Oberer M, Zechner R, Kohlwein SD, et al. Monoacylglycerol lipases act as evolutionarily conserved regulators of non-oxidative ethanol metabolism. *Journal of Biological Chemistry.* 2016;291(22):11865–11875. doi:10.1074/jbc.M115.705541.
- Gil-Ordóñez A, Martín-Fontecha M, Ortega-Gutiérrez S, López-Rodríguez ML. Monoacylglycerol lipase (MAGL) as a promising therapeutic target. *Biochem Pharmacol Cannabinoid Pharmacology and Therapeutics in Spain.* 2018;157:18–32. doi:10.1016/j.bcp.2018.07.036.
- Ali MR, Kumar S, Shalmali N, Afzal O, Azim S, Chanana D, Alam O, Paudel YN, Sharma M, Bawa S. Development of Thiazole-5-carboxylate derivatives as selective inhibitors of monoacylglycerol lipase as target in cancer. *Mini Rev Med Chem.* 2019;19(5):410–423. doi:10.2174/1389557518666180702103542.
- Koundouros N, Poulgiannis G. Reprogramming of fatty acid metabolism in cancer. *Br J Cancer.* 2020;122(1):4–22. doi:10.1038/s41416-019-0650-z.
- Nomura DK, Long JZ, Niessen S, Hoover HS, Ng S-W, Cravatt BF. Monoacylglycerol lipase regulates a fatty acid network that promotes cancer pathogenesis. *Cell.* 2010;140(1):49–61. doi:10.1016/j.cell.2009.11.027.
- Ye L, Zhang B, Seviour EG, Tao K, Liu X, Ling Y, Chen J, Wang G. Monoacylglycerol lipase (MAGL) knockdown inhibits tumor cells growth in colorectal cancer. *Cancer Lett.* 2011;307(1):6–17. doi:10.1016/j.canlet.2011.03.007.
- Ma M, Bai J, Ling Y, Chang W, Xie G, Li R, Wang G, Tao K. Monoacylglycerol lipase inhibitor JZL184 regulates apoptosis and migration of colorectal cancer cells. *Mol Med Rep.* 2016;13(3):2850–2856. doi:10.3892/mmr.2016.4829.
- Prüser JL, Ramer R, Wittig F, Ivanov I, Merkord J, Hinz B. The monoacylglycerol lipase inhibitor JZL184 inhibits lung cancer cell invasion and metastasis via the CB1 cannabinoid receptor. *Mol Cancer Ther.* 2021 Jan 1;20(5):787–802. doi:10.1158/1535-7163.MCT-20-0589.
- Baba Y, Funakoshi T, Mori M, Emoto K, Masugi Y, Ekmekcioglu S, Amagai M, Tanese K. Expression of monoacylglycerol lipase as a marker of tumour invasion and progression in malignant melanoma. *Journal of the European Academy of Dermatology and Venereology.* 2017;31(12):2038–2045. doi:10.1111/jdv.14455.
- Li X, Gao S, Li W, Liu Z, Shi Z, Qiu C, Jiang J. Effect of monoacylglycerol lipase on the tumor growth in endometrial cancer. *Journal of Obstetrics and Gynaecology Research.* 2019;45(10):2043–2054. doi:10.1111/jog.14070.
- Sun H, Jiang L, Luo X, Jin W, He Q, An J, Lui K, Shi J, Rong R, Su W, et al. Potential tumor-suppressive role of monoglyceride lipase in human colorectal cancer. *Oncogene.* 2013;32(2):234–241. doi:10.1038/onc.2012.34.
- Alhouayek M, Boldrup L, Fowler CJ. Altered mRNA expression of genes involved in endocannabinoid signalling in squamous cell carcinoma of the oral tongue. *Cancer Invest.* 2019;37(8):327–338. doi:10.1080/07357907.2019.1638394.
- Liu R, Wang X, Curtiss C, Landas S, Rong R, Sheikh MS, Huang Y. Monoglyceride lipase gene knockout in mice leads to increased incidence of lung adenocarcinoma. *Cell Death Dis.* 2018;9(2):1–15. doi:10.1038/s41419-017-0188-z.

28. Li C-F, Chuang I-C, Liu -T-T, Chen K-C, Chen -Y-Y, Fang F-M, Li S-H, Chen T-J, Yu S-C, Lan J, et al. Transcriptomic reappraisal identifies MGLL overexpression as an unfavorable prognosticator in primary gastrointestinal stromal tumors. *Oncotarget*. 2016;7(31):49986–49997. doi:10.18632/oncotarget.10304.
29. Zhang H, Guo W, Zhang F, Li R, Zhou Y, Shao F, Feng X, Tan F, Wang J, Gao S, et al. Monoacylglycerol lipase knockdown inhibits cell proliferation and metastasis in lung adenocarcinoma. *Front Oncol*. 2020;10. doi:10.3389/fonc.2020.559568.
30. Michalski CW, Oti FE, Erkan M, Sauliunaite D, Bergmann F, Pacher P, Batkai S, Müller MW, Giese NA, Friess H, et al. Cannabinoids in pancreatic cancer: correlation with survival and pain. *Int J Cancer*. 2008;122(4):742–750. doi:10.1002/ijc.23114.
31. Turcotte C, Chouinard F, Lefebvre JS, Flamand N. Regulation of inflammation by cannabinoids, the endocannabinoids 2-arachidonoyl-glycerol and arachidonoyl-ethanolamide, and their metabolites. *J Leukoc Biol*. 2015;97(6):1049–1070. doi:10.1189/jlb.3RU0115-021R.
32. Kienzl M, Kargl J, Schicho R. The immune endocannabinoid system of the tumor microenvironment. *Int J Mol Sci*. 2020;21(23):8929. doi:10.3390/ijms21238929.
33. Xiang W, Shi R, Kang X, Zhang X, Chen P, Zhang L, Hou A, Wang R, Zhao Y, Zhao K, et al. Monoacylglycerol lipase regulates cannabinoid receptor 2-dependent macrophage activation and cancer progression. *Nat Commun*. 2018;9(1):2574. doi:10.1038/s41467-018-04999-8.
34. Grill M, Hasenoehrl C, Kienzl M, Kargl J, Schicho R. Cellular localization and regulation of receptors and enzymes of the endocannabinoid system in intestinal and systemic inflammation. *Histochem Cell Biol*. 2019;151(1):5–20. doi:10.1016/S0009-3084(02)00150-0.
35. Tsukumo S, Yasutomo K. Regulation of CD8+ T cells and anti-tumor immunity by notch signaling. *Front Immunol*. 2018;9. doi:10.3389/fimmu.2018.00101.
36. Wölfel T, Klehmann E, Müller C, Schütt KH, Meyer zum Büschenfelde KH, Knuth A. Lysis of human melanoma cells by autologous cytolytic T cell clones. Identification of human histocompatibility leukocyte antigen A2 as a restriction element for three different antigens. *J Exp Med*. 1989;170(3):797–810. doi:10.1007/s00418-018-1719-0.
37. Mahmoud SMA, Paish EC, Powe DG, Macmillan RD, Grainge MJ, Lee AHS, Ellis IO, Green AR. Tumor-infiltrating CD8+ lymphocytes predict clinical outcome in breast cancer. *J Clin Oncol*. 2011;29(15):1949–1955. doi:10.1200/JCO.2010.30.5037.
38. Galon J, Costes A, Sanchez-Cabo F, Kirilovsky A, Mlecnik B, Lagorce-Pagès C, Tosolini M, Camus M, Berger A, Wind P, Zinzindohoué F, Bruneval P, Cugnenc PH, Trajanoski Z, Fridman WH, Pagès F. Type, density, and location of immune cells within human colorectal tumors predict clinical outcome. *Science*. 2006;313(5795):1960–4. doi:10.1126/science.1129139. PMID: 17008531.
39. Grisar-Tal S, Itan M, Klion AD, Munitz A. A new dawn for eosinophils in the tumour microenvironment. *Nat Rev Cancer*. 2020;20(10):594–607. doi:10.1038/s41568-020-0283-9.
40. Kienzl M, Hasenoehrl C, Valadez-Cosmes P, Maitz K, Sarsembayeva A, Sturm E, Heinemann A, Kargl J, Schicho R. IL-33 reduces tumor growth in models of colorectal cancer with the help of eosinophils. *OncoImmunology*. 2020;9(1):1776059. doi:10.1080/2162402X.2020.1776059.
41. Andreone S, Spadaro F, Buccione C, Mancini J, Tinari A, Sestili P, Gambardella AR, Lucarini V, Ziccheddu G, Parolini I, et al. IL-33 Promotes CD11b/CD18-mediated adhesion of eosinophils to cancer cells and synapse-polarized degranulation leading to tumor cell killing. *Cancers*. 2019;11(11):1664. doi:10.3390/cancers11111664.
42. Carretero R, Sektioglu IM, Garbi N, Salgado OC, Beckhove P, Hämmerling GJ. Eosinophils orchestrate cancer rejection by normalizing tumor vessels and enhancing infiltration of CD8+ T cells. *Nat Immunol*. 2015;16(6):609–617. doi:10.1038/ni.3159.
43. Chanda PK, Gao Y, Mark L, Btsh J, Strassle BW, Lu P, Piesla MJ, Zhang M-Y, Bingham B, Uveges A, et al. Monoacylglycerol lipase activity is a critical modulator of the tone and integrity of the endocannabinoid system. *Mol Pharmacol*. 2010;78(6):996–1003. doi:10.1124/mol.110.068304.
44. Guida M, Ligresti A, De Filippis D, D'Amico A, Petrosino S, Cipriano M, Bifulco G, Simonetti S, Orlando P, Insabato L, et al. The levels of the endocannabinoid receptor CB2 and its ligand 2-arachidonoylglycerol are elevated in endometrial carcinoma. *Endocrinology*. 2010;151(3):921–928. doi:10.1210/en.2009-0883.
45. Pagano E, Borrelli F, Orlando P, Romano B, Monti M, Morbidelli L, Aviello G, Imperatore R, Capasso R, Piscitelli F, et al. Pharmacological inhibition of MAGL attenuates experimental colon carcinogenesis. *Pharmacol Res*. 2017;119:227–236. doi:10.1016/j.phrs.2017.02.002.
46. Sailler S, Schmitz K, Jäger E, Ferreiros N, Wicker S, Zschiebsch K, Pickert G, Geisslinger G, Walter C, Tegeder I, et al. Regulation of circulating endocannabinoids associated with cancer and metastases in mice and humans. *Oncoscience*. 2014;1(4):272–282. doi:10.18632/oncoscience.33.
47. Grill M, Hogenauer C, Blesl A, Haybaeck J, Golob-Schwarzl N, Ferreiros N, Thomas D, Gurke R, Trotzmüller M, Kofeler HC, et al. Members of the endocannabinoid system are distinctly regulated in inflammatory bowel disease and colorectal cancer. *Sci.Rep*. 2019;9(1):235. doi:10.1038/s41598-019-38865-4.
48. Basu S, Dittel BN. Unraveling the complexities of cannabinoid receptor 2 (CB2) immune regulation in health and disease. *Immunol.Res*. 2011;51(1):26–38. doi:10.1007/s12026-011-8210-5.
49. Kaplan BL. The role of CB1 in immune modulation by cannabinoids. *Pharmacol.Ther*. 2013;137(3):365–374. doi:10.1016/j.pharmthera.2012.12.004.
50. Chouinard F, Lefebvre JS, Navarro P, Bouchard L, Ferland C, Lalancette-Hebert M, Marsolais D, Laviolette M, Flamand N. The endocannabinoid 2-arachidonoyl-glycerol activates human neutrophils: critical role of its hydrolysis and de novo leukotriene B4 biosynthesis. *J.Immunol*. 2011;186(5):3188–3196. doi:10.4049/jimmunol.1002853.
51. DeNardo DG, Andreu P, Coussens LM. Interactions between lymphocytes and myeloid cells regulate pro- versus anti-tumor immunity. *Cancer Metastasis Rev*. 2010;29(2):309–316. doi:10.1007/s10555-010-9223-6.
52. Busch SE, Hanke ML, Kargl J, Metz HE, MacPherson D, Houghton AM. Lung cancer subtypes generate unique immune responses. *J.I* 2016;197(11):4493–4503. doi:10.4049/jimmunol.1600576.
53. Leithner K, Wohlkoenig C, Stacher E, Lindenmann J, Hofmann NA, Gallé B, Guelly C, Quehenberger F, Stiegler P, Smolle-Jüttner F-M, et al. Hypoxia increases membrane metallo-endopeptidase expression in a novel lung cancer ex vivo model – role of tumor stroma cells. *BMC Cancer*. 2014;14(1):40. doi:10.1186/1471-2407-14-40.
54. Pfaffl MW. A new mathematical model for relative quantification in real-time RT-PCR. *Nucleic Acids Res*. 2001;29(9):e45. doi:10.1093/nar/29.9.e45.
55. Knuplez E, Curcic S, Theiler A, Bärnthaler T, Trakaki A, Trieb M, Holzer M, Heinemann A, Zimmermann R, Sturm EM, et al. Lysophosphatidylcholines inhibit human eosinophil activation and suppress eosinophil migration in vivo. *Biochimica Et Biophysica Acta (BBA) - Molecular and Cell Biology of Lipids*. 2020;1865(7):158686. doi:10.1016/j.bbalip.2020.158686.
56. Frei RB, Luschnig P, Parzmair GP, Peinhaupt M, Schranz S, Fauland A, Wheelock CE, Heinemann A, Sturm EM. Cannabinoid receptor 2 augments eosinophil responsiveness and aggravates allergen-induced pulmonary inflammation in mice. *Allergy*. 2016;71(7):944–956. doi:10.1111/all.12858.
57. Gurke R, Thomas D, Schreiber Y, Schäfer SMG, Fleck SC, Geisslinger G, Ferreiros N. Determination of endocannabinoids and endocannabinoid-like substances in human K3EDTA plasma – LC-MS/MS method validation and pre-analytical characteristics. *Talanta*. 2019;204:386–394. doi:10.1016/j.talanta.2019.06.004.
58. Hahnefeld L, Gurke R, Thomas D, Schreiber Y, Schäfer SMG, Trautmann S, Snodgrass IF, Kratz D, Geisslinger G, Ferreiros N.

- Implementation of lipidomics in clinical routine: can fluoride/citrate blood sampling tubes improve preanalytical stability? *Talanta*. 2020;209:120593. doi:10.1016/j.talanta.2019.120593.
59. Matyash V, Liebisch G, Kurzchalia TV, Shevchenko A, Schwudke D. Lipid extraction by methyl-tert-butyl ether for high-throughput lipidomics. *J Lipid Res*. 2008;49(5):1137–1146. doi:10.1194/jlr.D700041-JLR200.
60. Kind T, Liu K-H, Lee DY, DeFelice B, Meissen JK, Fiehn O. LipidBlast in silico tandem mass spectrometry database for lipid identification. *Nat Methods*. 2013;10(8):755–758. doi:10.1038/nmeth.2551.
61. Tang Z, Xie H, Heier C, Huang J, Zheng Q, Eichmann TO, Schoiswohl G, Ni J, Zechner R, Ni S, et al. Enhanced monoacylglycerol lipolysis by ABHD6 promotes NSCLC pathogenesis. *EBioMedicine*. 2020;53:102696. doi:10.1016/j.ebiom.2020.102696.
62. Chen Y, Ma Z, Zhong J, Li L, Min L, Xu L, Li H, Zhang J, Wu W, Dai L. Simultaneous quantification of serum monounsaturated and polyunsaturated phosphatidylcholines as potential biomarkers for diagnosing non-small cell lung cancer. *Sci Rep*. 2018;8(1):7137. doi:10.1038/s41598-018-25552-z.
63. Ros-Mazurczyk M, Jelonek K, Marczyk M, Binczyk F, Pietrowska M, Polanska J, Dziadziuszko R, Jassem J, Rzyman W, Widlak P. Serum lipid profile discriminates patients with early lung cancer from healthy controls. *Lung Cancer*. 2017;112:69–74. doi:10.1016/j.lungcan.2017.07.036.
64. Qiu C, Yang L, Wang B, Cui L, Li C, Zhuo Y, Zhang L, Zhang S, Zhang Q, Wang X. The role of 2-arachidonoylglycerol in the regulation of the tumor-immune microenvironment in murine models of pancreatic cancer. *Biomed.Pharmacother*. 2019;115 (JournalArticle):108952. doi:10.1016/j.biopha.2019.108952.
65. Oka S, Ikeda S, Kishimoto S, Gokoh M, Yanagimoto S, Waku K, Sugiura T. 2-arachidonoylglycerol, an endogenous cannabinoid receptor ligand, induces the migration of EoL-1 human eosinophilic leukemia cells and human peripheral blood eosinophils. *J Leukoc Biol*. 2004;76(5):1002–1009. doi:10.1189/jlb.0404252.
66. Ansari AM, Ahmed AK, Matsangos AE, Lay F, Born LJ, Marti G, Harmon JW, Cellular SZ. Cellular GFP toxicity and immunogenicity: potential confounders in in vivo cell tracking experiments. *Stem Cell Rev and Rep*. 2016;12(5):553–559. doi:10.1007/s12015-016-9670-8.
67. Siegel RL, Miller KD, Jemal A. Cancer statistics, 2020. *CA: A Cancer Journal for Clinicians*. 2020;70(1):7–30. doi:10.3322/caac.21590.
68. Alexander M, Kim SY, Cheng CH. Update 2020: management of non-small cell lung cancer. *Lung*. 2020 [2020];198(6):897–907. doi:10.1007/s00408-020-00407-5.
69. Kargl J, Busch SE, Yang GHY, Kim K-H, Hanke ML, Metz HE, Hubbard JJ, Lee SM, Madtes DK, McIntosh MW, et al. Neutrophils dominate the immune cell composition in non-small cell lung cancer. *Nat Commun*. 2017;8(1):14381. doi:10.1038/ncomms14381.
70. Winkler K, Ramer R, Dithmer S, Ivanov I, Merkord J, Hinz B. Fatty acid amide hydrolase inhibitors confer anti-invasive and antimetastatic effects on lung cancer cells. *Oncotarget*. 2016;7(12):15047–15064. doi:10.18632/oncotarget.7592.
71. Ravi J, Sneh A, Shilo K, Nasser MW, Ganju RK. FAAH inhibition enhances anandamide mediated anti-tumorigenic effects in non-small cell lung cancer by downregulating the EGF/EGFR pathway. *Oncotarget*. 2014;5(9):2475–2486. doi:10.18632/oncotarget.1723.
72. Preet A, Qamri Z, Nasser MW, Prasad A, Shilo K, Zou X, Groopman JE, Ganju RK, Receptors C. Cannabinoid Receptors, CB1 and CB2, as novel targets for inhibition of non-small cell lung cancer growth and metastasis. *Cancer Prev Res (Phila)*. 2011;4(1):65–75. doi:10.1158/1940-6207.CAPR-10-0181.
73. Xu S, Ma H, Bo Y, Shao M. The oncogenic role of CB2 in the progression of non-small-cell lung cancer. *Biomedicine & Pharmacotherapy*. 2019;117:109080. doi:10.1016/j.biopha.2019.109080.
74. Ravi J, Wani NA, Elbaz M, Nasser MW, Ganju RK. Cannabinoid receptor-2 agonist inhibits macrophage induced EMT in non-small cell lung cancer by downregulation of EGFR pathway. *Mol Carcinog*. 2016;55(12):2063–2076. doi:10.1002/mc.22451.
75. Zhang J, Liu Z, Lian Z, Liao R, Chen Y, Qin Y, Wang J, Jiang Q, Wang X, Gong J. Monoacylglycerol Lipase: a novel potential therapeutic target and prognostic indicator for hepatocellular carcinoma. *Sci Rep*. 2016;6. doi:10.1038/srep35784.
76. Prado-Garcia H, Romero-Garcia S, Aguilar-Cazares D, Meneses-Flores M, Lopez-Gonzalez JS. Tumor-Induced CD8+ T-cell dysfunction in lung cancer patients. *Clin Dev Immunol*. 2012 Oct 17. 2012; e741741. accessed December 7, 2020. <https://www.hindawi.com/journals/jir/2012/741741/>
77. Sheng SY, Gu Y, Lu CG, Zou JY, Hong H, Wang R. The distribution and function of human memory T cell subsets in lung cancer. *Immunol Res*. 2017;65(3):639–650. doi:10.1007/s12026-016-8882-y.
78. Simon S, Labarriere N. PD-1 expression on tumor-specific T cells: friend or foe for immunotherapy? *OncoImmunology*. 2018;7(1):e1364828. doi:10.1080/2162402X.2017.1364828.
79. Fernandez-Poma SM, Salas-Benito D, Lozano T, Casares N, Riezu-Boj J-I, Mancheño U, Elizalde E, Alignedani D, Zubeldia N, Otano I, et al. Expansion of tumor-infiltrating CD8+T cells Expressing PD-1 Improves the efficacy of adoptive T-cell therapy. *Cancer Res*. 2017;77(13):3672–3684. doi:10.1158/0008-5472.CAN-17-0236.
80. Taschler U, Eichmann TO, Radner FPW, Grabner GF, Wolinski H, Storr M, Lass A, Schicho R, Zimmermann R. Monoglyceride lipase deficiency causes desensitization of intestinal cannabinoid receptor type 1 and increased colonic  $\mu$ -opioid receptor sensitivity. *Br J Pharmacol*. 2015;172(17):4419–4429. doi:10.1111/bph.13224.
81. Turcotte C, Dumais É, Archambault AS, Martin C, Blanchet MR, É B, Boulet LP, Laviolette M, Di Marzo V, Flamand N. Human leukocytes differentially express endocannabinoid-glycerol lipases and hydrolyze 2-arachidonoyl-glycerol and its metabolites from the 15-lipoxygenase and cyclooxygenase pathways. *J.Leukoc.Biol*. 2019;106(6):1337–1347. doi:10.1002/JLB.3A0919-049RRR.
82. Varricchi G, Galdiero MR, Loffredo S, Lucarini V, Marone G, Mattei F, Marone G, Schiavoni G. Eosinophils: the unsung heroes in cancer? *Oncoimmunology*. 2017;7(2). doi:10.1080/2162402X.2017.1393134.
83. Stankovic B, Bjørhovde HAK, Skarshaug R, Aamodt H, Frafjord A, Müller E, Hammarström C, Beraki K, Bækkevold ES, Woldbæk PR, et al. Immune cell composition in human non-small cell lung cancer. *Front Immunol*. 2019;9. doi:10.3389/fimmu.2018.03101.
84. Hu W-R, Lian Y-F, Peng L-X, Lei J-J, Deng C-C, Xu M, Feng Q-S, Chen L-Z, Bei J-X, Zeng Y-X. Monoacylglycerol lipase promotes metastases in nasopharyngeal carcinoma. *Int J Clin Exp Pathol*. 2014;7:3704–3713.
85. Callejón-Leblic B, García-Barrera T, Grávalos-Guzmán J, Pereira-Vega A, Gómez-Ariza JL. Metabolic profiling of potential lung cancer biomarkers using bronchoalveolar lavage fluid and the integrated direct infusion/ gas chromatography mass spectrometry platform. *J Proteomics Focus on Medical Proteomics and Protein Quantitation*. 2016;145:197–206. doi:10.1016/j.jprot.2016.05.030.
86. Kargl J, Zhu X, Zhang H, Yang GHY, Friesen TJ, Shipley M, Maeda DY, Zebala JA, McKay-Fleisch J, Meredith G, et al. Neutrophil content predicts lymphocyte depletion and anti-PD1 treatment failure in NSCLC. *JCI Insight*. 2019;4(24):24. doi:10.1172/jci.insight.130850.